arXiv:cond-mat/0012222v1 [cond-mat.dis-nn] 13 Dec 2000

The Quantum Spherical p-Spin-Glass Model

Leticia F Cugliandolo[1,2], D. R. Grempel[3] and
Constantino A da Silva Santos[2]
[1]Laboratoire de Physique Théorique de l'École Normale Supérieure,
24 rue Lhomond, 75231 Paris Cedex 05, France
[2]Laboratoire de Physique Théorique et Hautes Énergies, Jussieu,
5ème étage, Tour 24, 4 Place Jussieu, 75252 Paris Cedex 05, France
[3]CEA-Service de Physique de l'État Condensé, CEA-Saclay,
91191 Gif-sur-Yvette CEDEX, France

February 1, 2008

Abstract

We study a quantum extension of the spherical p-spin-glass model using the imaginary-time replica formalism. We solve the model numerically and we discuss two analytical approximation schemes that capture most of the features of the solution. The phase diagram and the physical properties of the system are determined in two ways: by imposing the usual conditions of thermodynamic equilibrium and by using the condition of marginal stability. In both cases, the phase diagram consists of two qualitatively different regions. If the transition temperature is higher than a critical value $T^\star$, quantum effects are qualitatively irrelevant and the phase transition is *second* order, as in the classical case. However, when quantum fluctuations depress the transition temperature below $T^\star$, the transition becomes *first order*. The susceptibility is discontinuous and shows hysteresis across the first order line, a behavior reminiscent of that observed in the dipolar Ising spin-glass $LiHo_xY_{1-x}F_4$ in an external transverse magnetic field. We discuss in detail the thermodynamics and the stationary dynamics of both states. The spectrum of magnetic excitations of the equilibrium spin-glass state is gaped, leading to an exponentially small specific heat at low temperatures. That of the marginally stable state is gapless and its specific heat varies linearly with temperature, as generally observed in glasses at low temperature. We show that the properties of the marginally stable state are closely related to those obtained in studies of the real-time dynamics of the system weakly coupled to a quantum thermal bath. Finally, we discuss a possible application of our results to the problem of polymers in random media.

1 Introduction

The description of spin glasses in terms of classical statistical mechanics is generally justified since in most cases the transition temperature T_g is too high for quantum effects to be relevant. In some cases of practical interest, however, quantum fluctuations, controlled by an external parameter (*e.g.* magnetic field, doping, pressure), may reduce T_g down to arbitrarily low values and even suppress the glass transition altogether if they are strong enough. Among the experimental systems belonging to this class we may cite magnetic systems such as $LiHo_xY_{1-x}F_4$[1], $La_{2-x}Sr_xCuO_4$ [2] and $UCu_{5-x}Pd_x$ [3] as well as some randomly mixed hydrogen-bonded ferro-antiferroelectric crystals [4]. The theory of phase transitions in systems such as these must necessarily take into account their quantum mechanical nature.

A question of fundamental interest is whether there exists any *qualitative* differences between quantum spin-glass systems and their classical counterparts. This issue has been extensively investigated experimentally [1] in the case of the compound $LiHo_xY_{1-x}F_4$. This is a site-diluted derivative of the dipolar Ising ferromagnet $LiHoF_4$. For $x < 1$, the positional disorder of the magnetic Ho^{3+} ions makes the long range dipolar couplings random. $LiHo_xY_{1-x}F_4$ is thus a spin-glass with a freezing temperature $T_g(x)$ [1]. The application of an external magnetic field H *transverse* to the easy axis allows quantum tunneling through the barrier separating the two degenerate ground states of the Ho^{3+} ions. Quantum tunneling competes against spin freezing and the spin-glass ground state is expected to be destroyed at all temperatures if the tunneling frequency ($\propto H^2$) is sufficiently high. It was found experimentally that $LiHo_{0.167}Y_{0.833}F_4$ is paramagnetic at all temperatures above $H_c(0) \approx 12$ kOe [1]. Below this critical field, paramagnetic (PM) and spin-glass (SG) phases exist, separated by a line $H_c(T)$. Above 25 mK, the phase transition is second-order and signaled by a divergence of the non-linear susceptibility χ_3. However, below 25 mK, the divergence of χ_3 at the transition becomes a flat maximum at the position of which the imaginary part of the low-frequency linear susceptibility $\chi''(\omega)$ has a jump. These features strongly suggest that, at low transition temperatures [and in particular at the quantum critical point at $(H = H_c(0), T = 0)$] the transverse-field-induced spin-glass transition becomes *first order* [1]. This conclusion has recently received further support from the observation of hysteresis in the linear susceptibility measured as a function of the transverse field [5].

From the theoretical point of view, there is no evidence for this type of transition in the standard models for quantum spin glasses discussed in the literature. The quantum Edwards-Anderson (EA) [6] and Sherrington-Kirkpatrick (SK) [7, 8, 9] models are known to undergo second order transitions as also do models of metallic spin glasses [10]. Interestingly enough, this type of scenario does occur in less standard models with multi-spin interactions [11, 12, 13, 14, 15].

In this paper we study in detail the properties of one of these models, the p-spin spherical model with random interactions. We solve it using two different approaches. The first one consists in imposing the usual conditions of equilibrium to find the possible thermodynamic states of the system. In the second one, these are determined by imposing a condition of marginal stability. In both cases the problem

is solved using a 1-step replica symmetry breaking (RSB) *Ansatz* shown to be exact just as it is in the classical case. We find that, in terms of a quantum parameter Γ to be defined below, there is a line $\Gamma_c(T)$ in the $\Gamma - T$ plane that separates SG and PM phases. This line ends at a quantum critical point at $T = 0$, $\Gamma = \Gamma_c(0)$ above which the system is paramagnetic at all temperatures. Γ thus plays a role similar to that of the transverse field in the experiments described above. One of the main results of this paper is that a tricritical point $(T^\star, \Gamma^\star)$ divides the transition line in two sections. For $T \geq T^\star$, the SG transition is second order and the behavior of the quantum system is in all respects similar to that of the classical one. For $T < T^\star$, quantum fluctuations drive the transition first order. There is latent heat and the magnetic susceptibility is discontinuous and shows hysteresis across the first-order line. This is reminiscent of the behavior observed in $LiHo_xY_{1-x}F_4$ in a transverse magnetic field although, as it will be seen, important differences between the predictions of this model and experiment exist.

It should be noted that other quantum [11, 12] and classical [13, 14] models with similar characteristics were previously discussed in the literature but the connection with the experimental results was apparently not realized.

Several subtle points arise in this and related models [12, 13] when one has to choose between several possible equilibrium or marginally stable solutions. They stem from the existence of multiple stable PM and SG solutions in finite regions of phase space. To choose between them one has resort to physical arguments that go beyond the usual prescriptions of replica theory. We first show how this problem arises within an improved "static approximation" [7] that, despite its simplicity, contains the essential physics of the model. We then discuss it in the framework of the exact numerical solution of the model.

We investigate the *stationary* dynamics of the equilibrium and marginally stable SG states and show that they are quite different. We find that the magnetic excitation spectrum of the spin-glass state is gaped, leading to an exponentially small specific heat at low temperatures. The spectrum of the marginally stable state is gapless and its specific heat varies linearly with temperature. A power-law behavior of $C_v(T)$ is commonly observed in glasses at low-temperatures [16, 17] and is explained with models based on a distribution of two-level systems [18]. In this approach there are no such two-level systems but a linear $C_v(T)$ stems from the fact that the condition of marginal stability selects flat directions in phase space as opposed to the equilibrium condition that selects well-defined minima of the free-energy.

We show explicitly that the use of the condition of marginal stability in the Matsubara replica approach allows us to obtain, from a purely static calculation, partial information about the *non-equilibrium* real-time dynamics of the same system in contact with an environment, in the long-time, weak-coupling limits (taken in this order). We show that the transition line coincides with the dynamic transition line determined from the real-time formalism. We find that it also changes from second to first order at a tricritical point. This feature was also found in a study of the real-time dynamics of the model coupled to a bath where it is signaled by a jump in the asymptotic energy density when the system is driven across the

transition line [19]. We show that m, the break point in Parisi's RSB scheme, coincides with $T/T_{\rm EFF}$ [20], where T is the temperature of the quantum environment (that may be zero) and $T_{\rm EFF}$ is the dynamically generated effective temperature [21]. Finally, we demonstrate that the time-dependent correlation function calculated in the replica approach with the condition of marginal stability coincides, in the long waiting-time and weak-coupling limits, with the outcome of the dynamic calculation for the stationary part of the symmetrized correlation function [22]. As in the classical problem, equilibrium and marginal results can be interpreted in terms of the solutions of the TAP equations extended to include quantum fluctuations [23].

The paper is organized as follows. In Section 2 we present the model and derive its free-energy density with the Matsubara replica formalism. We discuss in detail several possible interpretations of the model and its relation to other ones that have already been studied. In Section 3 we introduce a refined static approximation which enables us to find the correct qualitative behavior of the system in the whole phase space. We analyze the consequences of using the static and marginal prescriptions for the spin-glass phase within this approximation. In Section 4 we present the exact numerical solution of the model distinguish again between the equilibrium and marginal cases. We also present a low-temperature, low-frequency approximate solution, that goes beyond the static approximation, and yields results for the real-frequency dependence of equilibrium correlation functions. The numerical results are presented in Section 5. The connection between our results and the real-time dynamics of the system is established in Section 6 where we compare the results for several quantities obtained in the static and dynamic formalisms. Finally, in Section 7 we draw our conclusions and we reinterpret our results for a classical polymer in a random media. We also briefly discuss related work in progress. A short account of some of our results appeared in Ref. [15].

2 The model

We study a quantum extension of the classical spherical p-spin-glass model [24] in which we reinterpret the continuous spins, s_i, as coordinate operators and introduce canonically conjugate momentum operators, π_i. Coordinate and momentum operators verify the usual commutation relations

$$[s_i, s_j] = [\pi_i, \pi_j] = 0 \ , \qquad [\pi_i, s_j] = -i\hbar\delta_{ij} \ . \tag{2.1}$$

The quantum spherical model is then defined by adding to the usual potential energy a "kinetic energy" term. The Hamiltonian reads

$$H[\vec{\pi}, \vec{s}, J] = \frac{\pi^2}{2M} + \sum_{i_1<\ldots<i_p}^{N} J_{i_1\ldots i_p} s_{i_1}\ldots s_{i_p} \ . \tag{2.2}$$

We denote $\pi^2 = \vec{\pi}\cdot\vec{\pi}$, $s^2 = \vec{s}\cdot\vec{s}$ with $\vec{\pi} = (\pi_1, \ldots, \pi_N)$ and $\vec{s} = (s_1, \ldots, s_N)$. A Lagrange multiplier z enforces the mean spherical constraint

$$\frac{1}{N}\sum_{i=1}^{N}\langle s_i^2\rangle = 1 \tag{2.3}$$

where the angular brackets denote the thermodynamic average.

The interaction strengths $J_{i_1 \ldots i_p}$ are taken from a Gaussian distribution with zero mean and variance

$$\overline{\left(J_{i_1 \ldots i_p}\right)^2} = \frac{\tilde{J}^2 p!}{2N^{p-1}} \, . \tag{2.4}$$

Hereafter the overline represents the average over disorder. The second term in the Hamiltonian is a random Gaussian potential energy with zero average and correlation

$$\overline{V(\vec{s})V(\vec{s}')} = \frac{\tilde{J}^2 N}{2} \left(\frac{\vec{s} \cdot \vec{s}'}{N} \right)^p \, . \tag{2.5}$$

2.1 Replica formalism

In order to study the static properties of the model we need to compute the disorder averaged free-energy density. The replica trick allows us to compute it as

$$\beta f = -\frac{1}{N} \overline{\ln Z} = -\frac{1}{N} \lim_{n \to 0} \frac{\overline{Z^n} - 1}{n}, \tag{2.6}$$

where the partition function, Z, is given by

$$Z = \mathrm{Tr} \; e^{-\beta H}. \tag{2.7}$$

In the Matsubara formalism, the disorder averaged replicated partition function can be written as a functional integral over replicated periodic functions of imaginary time, $\vec{s}_a(\tau)$, with $a = 1, \ldots, n$ being a replica index. These functions satisfy $\vec{s}_a(\beta\hbar) = \vec{s}_a(0)$. In order to decouple the p-interactions in the potential energy we introduce in $\overline{Z^n}$ the identity

$$\begin{aligned} 1 &\propto \int D\mathbf{Q} \; \delta \left(N Q_{ab}(\tau, \tau') - \vec{s}_a(\tau) \cdot \vec{s}_a(\tau') \right) \\ &\propto \int D\mathbf{Q} D\boldsymbol{\lambda} \; \exp \left[\frac{i}{2\hbar} \sum_{ab} \int_0^{\beta\hbar} d\tau \int_0^{\beta\hbar} d\tau' \lambda_{ab}(\tau, \tau') \left(N Q_{ab}(\tau, \tau') - \vec{s}_a(\tau) \cdot \vec{s}_b(\tau') \right) \right]. \end{aligned}$$

We shall hereafter use boldface to denote matrices in replica space. The averaged replicated partition function can be recast as

$$\overline{Z^n} = \int D\vec{s} D\boldsymbol{\lambda} D\mathbf{Q} \; \exp \left(-\frac{1}{\hbar} S_{\mathrm{EFF}} \right) \, , \tag{2.8}$$

with

$$\begin{aligned} -\frac{1}{\hbar} S_{\mathrm{EFF}} \;\; = \;\; & -\frac{1}{2} \sum_{ab} \int_0^{\beta\hbar} d\tau \int_0^{\beta\hbar} d\tau' \; \vec{s}_a(\tau) \cdot \left[\frac{i}{\hbar} O_{ab}(\tau - \tau') + \frac{i}{\hbar} \lambda_{ab}(\tau, \tau') \right] \vec{s}_b(\tau') \\ & + \frac{iN}{2\hbar} \sum_{ab} \int_0^{\beta\hbar} d\tau \int_0^{\beta\hbar} d\tau' \; \lambda_{ab}(\tau, \tau') Q_{ab}(\tau, \tau') + \frac{N\beta}{2} \sum_a z_a \\ & + \frac{\tilde{J}^2 N}{4\hbar^2} \sum_{ab} \int_0^{\beta\hbar} d\tau \int_0^{\beta\hbar} d\tau' \; Q_{ab}^{\bullet p}(\tau, \tau') \, . \end{aligned} \tag{2.9}$$

We denote with a bullet the usual product: $Q_{ab}^{\bullet p}(\tau) = Q_{ab}(\tau)\cdots Q_{ab}(\tau)$, p times, to distinguish it from the operational product. O_{ab} is a short-hand notation for the differential operator

$$O_{ab}(\tau-\tau') = i\delta_{ab}\delta(\tau-\tau')\left(M\frac{\partial^2}{\partial\tau^2} - z_a\right) . \tag{2.10}$$

It follows that, at the saddle-point, the expectation value of the order-parameter $Q_{ab}(\tau,\tau')$ is given by

$$Q_{ab}(\tau,\tau') = \frac{1}{N}\overline{\langle\vec{s}_a(\tau)\cdot\vec{s}_b(\tau')\rangle} , \tag{2.11}$$

with $Q_{ab}(\tau,\tau')$ periodic in τ and τ' with period $\beta\hbar$. The mean spherical constraint reads $Q_{aa}(\tau,\tau) = 1$ for all τ.

Since we are studying an equilibrium problem, all correlation functions are time-translational invariant. They are also symmetric in imaginary time due to the time-reversal invariance of the Hamiltonian:

$$Q_{ab}(\tau,\tau') = Q_{ab}(\tau-\tau') = Q_{ab}(\tau'-\tau) , \quad \lambda_{ab}(\tau,\tau') = \lambda_{ab}(\tau-\tau') = \lambda_{ab}(\tau'-\tau) . \tag{2.12}$$

Using these properties we can simplify the effective action and write it as

$$\begin{aligned} -\frac{1}{\hbar}S_{\rm EFF} = &-\frac{1}{2}\sum_{ab}\int_0^{\beta\hbar}d\tau\int_0^{\beta\hbar}d\tau'\ \vec{s}_a(\tau)\cdot\left[\frac{i}{\hbar}O_{ab}(\tau-\tau') + \frac{i}{\hbar}\lambda_{ab}(\tau-\tau')\right]\vec{s}_b(\tau') \\ &+\frac{iN\beta}{2}\sum_{ab}\int_0^{\beta\hbar}d\tau\,\lambda_{ab}(\tau)Q_{ab}(\tau) + \frac{\tilde{J}^2N\beta}{4\hbar}\sum_{ab}\int_0^{\beta\hbar}d\tau\,Q_{ab}^{\bullet p}(\tau) + \frac{Nn\beta}{2}z , \end{aligned} \tag{2.13}$$

where we have further assumed that z_a does not depend on the replica index. In the following, we work with the Fourier transforms

$$\begin{aligned} \tilde{s}_i(\omega_k) &= \frac{1}{\sqrt{\beta\hbar}}\int_0^{\beta\hbar}d\tau e^{i\omega_k\tau}s_i(\tau) , \\ s_i(\tau) &= \frac{1}{\sqrt{\beta\hbar}}\sum_k e^{-i\omega_k\tau}\tilde{g}_i(\omega_k) , \end{aligned} \tag{2.14}$$

with the Matsubara frequencies given by

$$\omega_k = \frac{2\pi k}{\beta\hbar} \qquad k = 0, \pm1, \ldots . \tag{2.15}$$

This implies

$$\tilde{Q}_{ab}(\omega_k) = \int_0^{\beta\hbar}d\tau\, exp(i\omega_k\tau)\, Q_{ab}(\tau) , \tag{2.16}$$

$$Q_{ab}(\tau) = (\beta\hbar)^{-1}\sum_k exp(-i\omega_k\tau)\,\tilde{Q}_{ab}(\omega_k) . \tag{2.17}$$

In terms of the Fourier transformed variables the effective action reads

$$-\frac{1}{\hbar}S_{\rm EFF} = -\frac{1}{2}\sum_k\sum_{ab}\tilde{\vec{s}}_a(-\omega_k)\cdot\left[\frac{i}{\hbar}\tilde{O}_{ab}(\omega_k)+\frac{i}{\hbar}\tilde{\lambda}_{ab}(\omega_k)\right]\tilde{\vec{s}}_b(\omega_k)+\frac{Nn\beta}{2}z$$
$$+\frac{iN}{2\hbar}\sum_k\sum_{ab}\tilde{\lambda}_{ab}(\omega_k)\tilde{Q}_{ab}(\omega_k)+\frac{\tilde{J}^2N\beta}{4\hbar}\sum_{ab}\int_0^{\beta\hbar}d\tau\left(\frac{1}{\hbar\beta}\sum_k\exp(-i\omega_k\tau)\tilde{Q}_{ab}(\omega_k)\right)^p \tag{2.18}$$

where we used $\tilde{Q}_{ab}(\omega_k)=\tilde{Q}_{ab}(-\omega_k)$. The functional integration over the functions $\tilde{\vec{s}}(\omega_k)$ is quadratic and can be explicitly performed. This amounts to replace the quadratic term in the action by

$$-\frac{N}{2}\sum_k{\rm Tr}\ln\left[i\beta\left(\tilde{\mathbf{O}}(\omega_k)+\tilde{\boldsymbol{\lambda}}(\omega_k)\right)\right]. \tag{2.19}$$

where we took into account a factor $(\beta\hbar)^{-n/2}$ that comes from the change in variables $\vec{s}_a(\tau)\rightarrow\tilde{\vec{s}}_a(\omega_k)$ in the partition function. The trace is to be taken over replica indices.

The effective action is now proportional to N and, in the large N limit, this allows us to evaluate the replicated partition function by the steepest descent method. The saddle-point equation with respect to $\tilde{\lambda}_{ab}(\omega_k)$ reads

$$\frac{i}{\hbar}\tilde{\mathbf{Q}}=\left(\tilde{\mathbf{O}}+\tilde{\boldsymbol{\lambda}}\right)^{-1}. \tag{2.20}$$

By replacing this value of $\tilde{\lambda}_{ab}(\omega_k)$ in (2.18) one obtains

$$\begin{aligned}-\frac{1}{\hbar}S_{\rm EFF} &= \frac{N}{2}\sum_k{\rm Tr}\ln\left((\beta\hbar)^{-1}\tilde{\mathbf{Q}}\right)+\frac{N}{2}\sum_k\left(n-\frac{i}{\hbar}\sum_{ab}\tilde{O}_{ab}(\omega_k)\tilde{Q}_{ab}(\omega_k)\right)\\ &+\frac{\tilde{J}^2N\beta}{4\hbar}\sum_{ab}\int_0^{\beta\hbar}d\tau\left(\frac{1}{\hbar\beta}\sum_k\exp(-i\omega_k\tau)\tilde{Q}_{ab}(\omega_k)\right)^p+\frac{Nn\beta}{2}z\end{aligned} \tag{2.21}$$

Finally, the averaged replicated partition function as a function of $\tilde{\mathbf{Q}}$ becomes

$$\overline{Z^n}=\exp\left(-nNG_0\right) \tag{2.22}$$

where

$$\begin{aligned}2G_0 &= -\frac{1}{n}\sum_k{\rm Tr}\ln\left((\beta\hbar)^{-1}\tilde{\mathbf{Q}}\right)-\sum_k\left(1-\frac{i}{n\hbar}\sum_{ab}\tilde{O}_{ab}(\omega_k)\tilde{Q}_{ab}(\omega_k)\right)\\ &-\frac{\tilde{J}^2\beta}{2\hbar n}\sum_{ab}\int_0^{\beta\hbar}d\tau\left(\frac{1}{\hbar\beta}\sum_k\exp(-i\omega_k\tau)\tilde{Q}_{ab}(\omega_k)\right)^p-\beta z\end{aligned} \tag{2.23}$$

and the free-energy per spin is

$$\beta f=\lim_{n\rightarrow0}G_0\,. \tag{2.24}$$

The saddle-point equation with respect to the order parameter $\tilde{Q}_{ab}(\omega_k)$ reads

$$\frac{1}{\hbar}(M\omega_n^2 + z)\delta_{ab} = \left(\tilde{\mathbf{Q}}^{-1}\right)_{ab}(\omega_k) + \frac{\tilde{J}^2 p}{2\hbar^2}\int_0^{\hbar\beta} d\tau \exp(i\omega_k\tau) Q_{ab}^{\bullet p-1}(\tau), \tag{2.25}$$

that transforming back to imaginary time becomes

$$-\frac{1}{\hbar}\left(M\frac{\partial^2}{\partial\tau^2} - z\right)\delta_{ab}\delta(\tau) = Q_{ab}^{-1}(\tau) + \frac{\tilde{J}^2 p}{2\hbar^2} Q_{ab}^{\bullet p-1}(\tau)\ . \tag{2.26}$$

Equation (2.26) together with the spherical constraint

$$Q_{aa}(0) = 1, \qquad \frac{1}{\beta\hbar}\sum_k \tilde{Q}_{aa}(\omega_k) = 1\ , \tag{2.27}$$

are the equations that characterize the different phases of the model.

From here on, we shall work with dimensionless quantities. We take $\tilde{J}$ as the unit of energy and $\hbar/\tilde{J}$ as the unit of time. Hence, we redefine the imaginary time and Matsubara frequencies as

$$\hat{\tau} \equiv \frac{\tilde{J}\tau}{\hbar} \ \Rightarrow\ \hat{\omega}_k \equiv \frac{\hbar\omega_k}{\tilde{J}}\ . \tag{2.28}$$

The Lagrange multiplier is now given by $\hat{z} = z/\tilde{J}$ and, consequently, Eq. (2.26) becomes

$$\left(-\frac{1}{\Gamma}\frac{\partial^2}{\partial\tau^2} + z\right) Q_{ab}(\tau) = \delta_{ab}(\tau) + \sum_c \int_0^\beta d\tau'\, \frac{p}{2} Q_{ac}^{\bullet p-1}(\tau - \tau') Q_{cb}(\tau')\ , \tag{2.29}$$

where $\Gamma = \hbar^2/(M\tilde{J})$ and we have eliminated all hats in order to simplify the notation.

The matrix elements $Q_{ab}(\tau)$ are the order parameters of the model. The diagonal components $Q_{aa}(\tau) = N^{-1}\overline{\langle \vec{s}_a(\tau)\cdot\vec{s}_a(0)\rangle}$ in Eq. (2.29) have no classical analog. Indeed, in the classical limit $0 \le \tau \le \hbar\beta$ and $\lim_{\hbar\to 0} Q_{aa}(\tau) = Q_{aa}(0) \equiv 1$ on account of the constraint (2.3). In the quantum mechanical case $Q_{aa}(\tau)$ encodes information about the equilibrium dynamics of the system through its connection to the dynamic local susceptibility $\chi(\omega)$,

$$Q_{aa}(\tau) = \int_{-\infty}^{\infty}\frac{d\omega}{\pi}\chi''(\omega)\frac{\exp(-\omega|\tau|)}{1-\exp(-\beta\omega)}\ , \tag{2.30}$$

where $\chi''(\omega) = \mathrm{Im}\chi(\omega)$. It follows that $\tilde{Q}_{aa}(i\omega_k) = \chi(\omega)|_{\omega+i\epsilon\to i\omega_k}$ and $Q_{aa} = C(t)|_{t\to -i\tau}$, where C is the real-time autocorrelation function [22]. We shall hereafter use the notation $Q_{aa}(\tau) = q_d(\tau)$.

The off-diagonal elements Q_{ab} are τ-independent. This is a general and important property of quantum disordered systems in equilibrium proven by Bray and Moore in their pioneering work on quantum spin-glasses [7]. The argument goes as follows. The overlap matrix for $a \neq b$ is

$$NQ_{a\neq b}(\tau,\tau') = \overline{\langle \vec{s}_a(\tau)\cdot\vec{s}_b(\tau')\rangle}\ . \tag{2.31}$$

Before performing the average over disorder, replicas are decoupled and the thermal average factorizes. But the averages $\langle s_a(\tau)\rangle$ are time-independent for any fixed configuration of disorder and so is the average of their product. Consequently, the Fourier transform of $Q_{a\neq b}(\tau) = q_{a\neq b}$ is given by

$$\tilde{q}_{a\neq b} = q_{a\neq b}\hbar\beta\delta_{\omega_k,0}. \tag{2.32}$$

We conclude that the RSB solution is confined to the zero mode of the Matsubara frequencies and that $q_{a\neq b}$ is the quantum analog of the classical order-parameter matrix.

2.2 Relationships to other models

Besides being a quantum extension of the spherical p spin-glass this model can be interpreted in other ways. First, if we identify $\vec{s} = (s_1, s_2, \ldots, s_N)$ as a position vector in N-dimensional space, Hamiltonian (2.2) with the constraint (2.3) describes the motion of a quantum particle of mass M constrained to move on the N-hypersphere of radius $\sqrt{N}$ in the presence of a random potential $V(\vec{s})$ with p-dependent correlations given by Eq. (2.5).

Second, the well known connection between quantum mechanics in D dimensions and statistical mechanics in $D+1$ dimensions allows us to interpret this model as representing a classical closed polymer in a quenched random medium in infinite transverse dimensions [27, 25, 26]. The imaginary time τ represents the internal coordinate of the polymer of contour length $L = \beta\hbar$. The low temperature limit of the quantum model corresponds then to the long length limit of the polymer. The N components of the field $\vec{s}$ denote the N transverse coordinates on the spherical embedding space. The parameter Γ is a measure of the linear elasticity of the polymer since the first term on the left-hand-side of Eq. (2.29) may be thought of as deriving from an elastic energy. Finally, the last interaction term is a consequence of the average over the quenched disorder. The time-dependent replica matrix $Q_{ab}(\tau)$ quantifies the correlation between the position of different monomers, τ being the distance between them, measured following the polymer direction. The replica indices represent different states of the polymer.

There are also several quantum models related to this one. When $p = 2$ one recovers the model studied in Ref. [28] as well as the disordered quantum-rotor model of Ref. [29]. Quantum Ising spin models with p-spin interactions in a transverse field have been extensively studied in the literature [11, 12, 30]. A different quantization rule for spherical spins was proposed in Ref. [31] and it was later studied in detail, including p-spin interactions, in Ref. [12]. The difference in the quantization rule results in a different imaginary-time dynamics as the equation of motion contains first-order imaginary-time derivatives instead of second-order ones as we have here.

Notice that if we set $p = 4$, Eq. (2.29) becomes similar to Eqs. (4)-(6) in Ref. [32] for the replicated boson Green's function $G_{ab}(\tau)$ in the SU($\mathcal{N}$) Heisenberg spin-glass model. Indeed, the equations look identical if we formally take $S = -1$, redefine J and replace the term linear in the Matsubara frequencies by a quadratic one, *i.e.*, if we use first-order instead of second-order imaginary-time derivatives. Note,

however, that the symmetry properties of the quantities G (in Ref. [32]) and Q (here) are quite different.

Chandra *et al.* showed the equivalence between a model for a classical array of Josephson junctions in a magnetic field and the p-spin-glass model with $p = 4$ [38]. Using a diagrammatic expansion technique similar to that used to derive classical or quantum TAP equations, Kagan *et al.* [37] showed that the equations governing the equilibrium behavior of the quantized model are similar, though not identical, to the Matsubara equations we analyze here.

3 The static approximation

Before presenting the full numerical solution of the model it is useful to study it using a very simple approximation known as the static approximation. The latter, first introduced as a variational *Ansatz* in Ref. [7], consists in proposing $q_d(\tau) \equiv q_d$, independent of τ, and determining q_d by minimization of the free-energy. Despite its simplicity, detailed comparison with exact numerical results [9, 12] has shown that the static approximation captures much of the physics of quantum spin mean-field models. In our case, however, the naïve static approximation applied at the level of the saddle point equations is oversimplified since the spherical constraint (2.27) immediately sets $q_d = 1$ thus loosing all variational freedom. We then proceed differently and replace $q_d(\tau)$ by q_d and $\lambda_d(\tau)$ by λ_d at the level of the effective action (2.9) and treat both quantities as variational parameters. In this way, we do not impose the spherical constraint strictly (since q_d can be different from 1) but in an averaged manner.

The effective action in the static approximation becomes

$$\begin{aligned} -\frac{1}{\hbar} S_{\text{EFF}} &= \frac{N}{2}\text{Tr}\ln\mathbf{Q} - \frac{Nn}{2}\sum_{k\neq 0}\ln\left[\beta\left(\frac{\omega_k^2}{\Gamma}+z\right)\right] + \frac{N\beta^2}{4}\sum_{ab}Q_{ab}^{\bullet p} \\ &\quad + \frac{Nn}{2}\left(1+\beta z(1-q_d)\right) \ . \end{aligned} \tag{3.1}$$

By using the identity [33]

$$\sum_k \ln\left[\beta\left(\frac{\omega_k^2}{\Gamma}+z\right)\right] = 2\ln\left[2\sinh\left(\frac{\beta\sqrt{\Gamma z}}{2}\right)\right] \ , \tag{3.2}$$

we get the following expression for the free-energy density

$$\begin{aligned} \beta f &= -\frac{1}{2}\ln(\beta z) + \ln\left[2\sinh\left(\frac{\beta\sqrt{\Gamma z}}{2}\right)\right] - \lim_{n\to 0}\frac{1}{n}\left[\frac{1}{2}\text{Tr}\ln\mathbf{Q} + \frac{\beta^2}{4}\sum_{ab}Q_{ab}^{\bullet p}\right] \\ &\quad -\frac{1}{2}\left(1+\beta z(1-q_d)\right) \ . \end{aligned} \tag{3.3}$$

The saddle-point equation with respect to z reads

$$q_d = 1 + \frac{1}{\beta z} - \frac{1}{2}\sqrt{\frac{\Gamma}{z}}\coth\left(\frac{\beta}{2}\sqrt{\Gamma z}\right) \tag{3.4}$$

and replaces the spherical constraint. As expected, it is independent of the non-diagonal part of the $\mathbf{Q}$ matrix. At high temperature ($\beta \to 0$) one recovers the classical result, $q_d \equiv 1$. In the opposite limit, $\beta \to \infty$,

$$q_d \to 1 - \frac{1}{2}\sqrt{\frac{\Gamma}{z}} \; . \tag{3.5}$$

The second term on the right hand side of the equation corresponds to the zero-point reduction of the order parameter characteristic of quantum magnets.

The saddle-point equation with respect to the order-parameter Q_{ab} is

$$z\delta_{ab} = \frac{1}{\beta} Q^{-1}_{ab} + \frac{p\beta}{2} Q^{\bullet p-1}_{ab} \; . \tag{3.6}$$

3.1 The paramagnetic solution

At high temperatures or if quantum fluctuations are strong we expect a PM phase. Within the static approximation, the PM solution is associated to a diagonal replica matrix $\mathbf{Q}$:

$$Q_{ab}(\tau) = q_d \delta_{ab} \; . \tag{3.7}$$

The saddle-point equation (3.6) is now very simple

$$z \;\; = \;\; \frac{1}{\beta q_d} + \frac{p\beta}{2} q_d^{p-1} \; . \tag{3.8}$$

This equation and Eq. (3.4) form a set of two coupled equations for q_d and z that can be solved numerically for all β and Γ.

Some asymptotic behaviors can be obtained analytically. First, in the classical limit, T fixed and $\Gamma \to 0$, Eqs. (3.6) and (3.8) imply $q_d = 1$ and $\beta z = 1 + p\beta^2/2$, in agreement with the results in Ref. [24]. Second, when $T \gg 1$ but $\beta\Gamma \ll 1$, quantum fluctuations are still irrelevant and we get $\beta z = 1$ and $q_d = 1$. Third, in the limit $\Gamma \to \infty$ and T finite, q_d tends to zero as $q_d \sim 4/(\beta\Gamma)$ and $z \sim \Gamma/4$. The zero-temperature limit is more subtle and we discuss it below.

The properties of the general solution of Eqs. (3.6) and (3.8) are best understood graphically. In Figs. 1(a) and (b) we display $g(q_d) \equiv q_d -$ rhs(Eq. (3.4)) *vs.* q_d, obtained replacing z by its value given by Eq. (3.8), for several values of T and Γ. The points where $g(q_d)$ crosses the horizontal axis are the solutions for q_d.

The summary of our results for $p \geq 3$ is the following (the case $p = 2$ is different and we discuss it in Section 3.3):

- For fixed $\beta < \beta_{\rm P}$ (≈ 6 for $p = 3$) and all values of Γ, the equations admit only one solution with $0 \leq q_d \leq 1$. The function $q_d(\Gamma)$ decreases monotonically with $q_d(0) = 1$ and $q_d \to 0$ when $\Gamma \to \infty$. This is represented in Fig. 1 (a), where we show $g(q_d)$ for $\beta = 1 < \beta_{\rm P}$ and $\Gamma = 0.1, 10, 100$. The analysis of the free-energy density shows that this solution is a local minimum of $f(q_d)$.

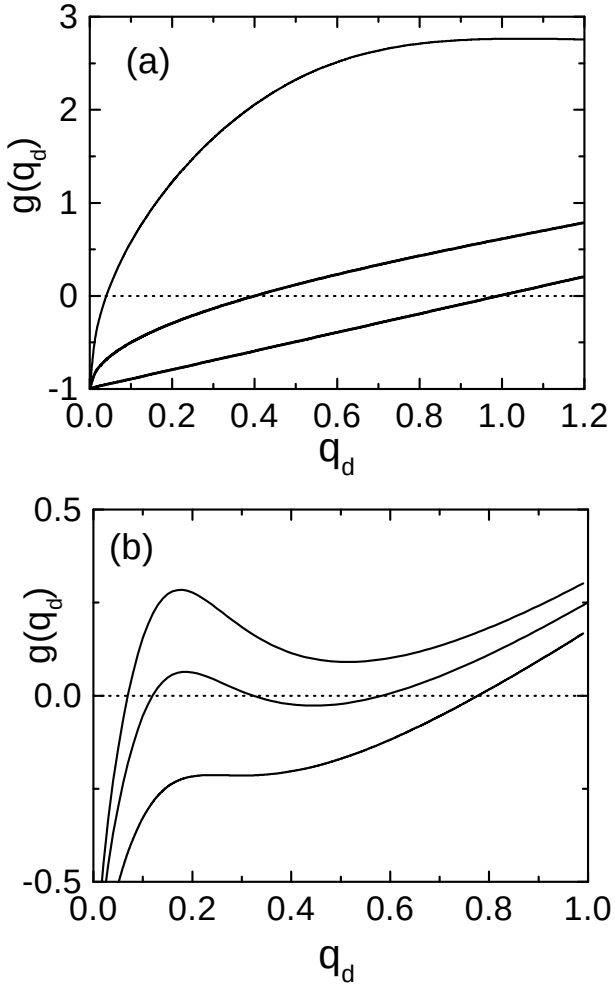

Figure 1: (a): The function $g(q_d)$ that determines the PM solutions for $\beta = 1 < \beta_{\rm P} \approx 6$ and $\Gamma = 0.1, 10, 100$, from bottom to top. For all Γ we find only one solution that moves towards smaller values of q_d when Γ increases. (b): The same for $\beta = 10 > \beta_{\rm P} \approx 6$ and several choices of Γ. For $\Gamma = 6 > \Gamma_{c1}$ (top curve) there is only one solution with a small value of q_d; for $\Gamma_{c2} < \Gamma = 4 < \Gamma_{c1}$ (middle curve) there are three solutions, while for $\Gamma = 2 < \Gamma_{c2}$ (lower curve) there is again only one solution but with a large value of q_d.

- For $\beta > \beta_{\rm P}$, there are several PM solutions and phase transitions can occur between them upon varying Γ. For Γ above a critical value Γ_{c1}, there exists a solution $\rm PM_1$ with a small value of $q_d = q_d^<$ (the upper curve in Fig. 1(b)) that we call a quantum paramagnet. This solution can be continued below Γ_{c1} but two new ones appear: $\rm PM_2$, that we call a classical paramagnet, with large $q_d = q_d^>$, and $\rm PM_3$ with an intermediate value of q_d. The three solutions coexist in the interval $\Gamma_{c2} < \Gamma < \Gamma_{c1}$. At Γ_{c2}, $\rm PM_1$ and $\rm PM_3$ merge and disappear. The three coexisting solutions are shown in the intermediate curve in Fig. 1(b). Below Γ_{c2}, only $\rm PM_2$ exists (the lower curve in Fig. 1(b)). An analysis of the stability of these solutions shows that, where they exist, $\rm PM_1$ and $\rm PM_2$ are local minima of the free-energy whereas $\rm PM_3$ is a local maximum and can therefore be immediately discarded. In the limit $\beta \to \infty$ the two stable solutions can be simply computed and one obtains $q_d^> \sim 1 - \sqrt{\Gamma/(2p)}\beta^{-1/2} \to 1$ with $z \sim p\beta/2$ and $q_d^< \sim 4/(\Gamma\beta) \to 0$ with $z \sim \Gamma/4$. Both solutions exist for all values of Γ when $T \to 0$, indicating that $\Gamma_{c1} \to \infty$ and $\Gamma_{c2} \to 0$ as $T \to 0$. The dotted lines in Fig. 5 delimit the region where there is coexistence of paramagnetic solutions in the case $p = 3$.

- The free-energies of the two stable PM solutions cross at Γ_{c0}, a coupling intermediate between Γ_{c1} and Γ_{c2}. For $\Gamma > \Gamma_{c0}$, $f(q_d^<) < f(q_d^>)$ but the inequality is reversed for $\Gamma < \Gamma_{c0}$. This would suggest that, for all $0 \leq T \leq T_{\rm P}$, there is a first-order transition between the two stable PM states with $\rm PM_2$ favored for $\Gamma < \Gamma_{c0}$. However, we will see below that this transition is only possible for $T^\star \leq T \leq T_{\rm P}$ where $T^\star$ is slightly below $T_{\rm P}$ for small to moderate p.

3.2 The SG solution

3.2.1 The replica symmetric solution

At low temperatures one expects the system to exhibit a non trivial SG solution characterized by a replica matrix with non-vanishing off-diagonal elements. The simplest possible *Ansatz* is the replica-symmetric (RS) one,

$$Q_{ab} = (q_d - q_{\rm EA})\delta_{ab} + q_{\rm EA}. \tag{3.9}$$

From the general expression (3.3) for the free-energy one then derives three equations for z, q_d and $q_{\rm EA}$. The equation for z is independent of the *Ansatz* and hence coincides with Eq. (3.4). The other two equations read

$$z = \frac{1}{\beta}\frac{q_d - 2q_{\rm EA}}{(q_d - q_{\rm EA})^2} + \frac{\beta p}{2} q_d^{p-1}\,, \tag{3.10}$$

$$0 = -\frac{1}{(q_d - q_{\rm EA})^2} + \frac{p\beta^2}{2} q_{\rm EA}^{p-2}\,, \tag{3.11}$$

after we eliminated the paramagnetic solution $q_{\rm EA} = 0$.

These equations have non-trivial solutions in a finite region of phase space satisfying $0 \leq q_{\rm EA} \leq q_d$. The phenomenon of multiplicity of solutions at low temperatures

found in the PM case appears also here. For temperatures that are not too low, (*e.g.* for $\beta = 10$ for $p = 3$), these equations have two solutions, one stable and one unstable *within* the RS *Ansatz*. At very low temperatures, two other solutions appear, one stable and one unstable within RS. However, a careful analysis of stability shows that, as in the classical case [24], the RS solutions are always *unstable* with respect to replica symmetry breaking. To show this, it is sufficient to compute the *replicon* Λ_T, the transverse eigenvalue of the Hessian matrix . We will derive a general expression for Λ_T in Section 4.4.1. Here we simply quote the result in the static approximation which is

$$\Lambda_T = \frac{1}{(q_d - q_{\rm EA})^2} - \frac{\beta^2}{2} p(p-1) q_{\rm EA}^{p-2}. \tag{3.12}$$

It follows from this equation and Eq. (3.11) that Λ_T cannot be positive for any of the RS solutions if $p \geq 3$. (See Section 3.3 for a discussion of the case $p = 2$.)

3.2.2 The 1-step replica symmetry breaking solution

Using Parisi's RSB scheme, we search now for a 1-step (RSB) solutions of the form

$$Q_{ab} = (q_d - q_{\rm EA})\delta_{ab} + (q_{\rm EA} - q_0)\epsilon_{ab} + q_0 \ , \tag{3.13}$$

where the matrix ϵ is defined as

$$\epsilon_{ab} = \begin{cases} 1 & \text{if } a \text{ and } b \text{ are in a diagonal block} \\ 0 & \text{otherwise} \end{cases} \tag{3.14}$$

We show in the Appendix that this *Ansatz* actually gives the exact solution to the full problem. In the absence of an external magnetic field $q_0 = 0$ and the extremization equations with respect to q_d, $q_{\rm EA}$ and m read

$$\beta z = \frac{q_d + (m-2)q_{\rm EA}}{(q_d - q_{\rm EA}(1-m))(q_d - q_{\rm EA})} + \frac{p\beta^2}{2} q_d^{p-1} \ , \tag{3.15}$$

$$0 = \frac{1}{(q_d - q_{\rm EA}(1-m))(q_d - q_{\rm EA})} - \frac{p\beta^2}{2} q_{\rm EA}^{p-2} \ , \tag{3.16}$$

$$0 = \frac{p q_{\rm EA}}{m(q_d - q_{\rm EA}(1-m))} + \frac{p}{m^2} \ln\left(\frac{q_d - q_{\rm EA}}{q_d - q_{\rm EA}(1-m)}\right) + \frac{p\beta^2}{2} q_{\rm EA}^{p} \ , \tag{3.17}$$

where we excluded the two solutions $m = 1$ or $q_{\rm EA} = 0$ from Eq. (3.16). The first and second equations above have new m-dependent factors. These equations reduce to the RS equations when $m = 0$. The third equation is new and is used to determine the break point m.

It is useful to define the parameters

$$y = \frac{q_{\rm EA}}{q_d} \ , \qquad x_p = \frac{my}{1-y} \ , \tag{3.18}$$

Subtracting Eq. (3.17) from Eq. (3.16) and writing the result in terms of x_p one obtains

$$\ln\left(\frac{1}{1+x_p}\right) + \frac{x_p}{1+x_p} + \frac{x_p^2}{p(1+x_p)} = 0 \; . \tag{3.19}$$

This is a master equation for x_p that only depends on the parameter p. Once x_p is known from this equation, y follows from $y = x_p/(m+x_p)$. For $p = 3$, a case that we will consider in detail

$$x_3 = 1.81696 \tag{3.20}$$

Equation (3.16) yields a simple relation between $q_{\rm EA}$ and x_p. Using then $q_{\rm EA} = x_p/(m+x_p)q_d$ one has

$$\frac{p(m\beta)^2}{2} q_{\rm EA}^p = \frac{x_p^2}{1+x_p} \; , \tag{3.21}$$

$$\frac{p(m\beta)^2}{2} q_d^p = \frac{x_p^{2-p}(m+x_p)^p}{1+x_p} \; . \tag{3.22}$$

For fixed values of m and β, one obtains $q_{\rm EA}$, q_d and z from Eqs. (3.21), (3.22) and (3.15), respectively. Solving numerically Eq. (3.4) one gets the corresponding value of Γ.

To study the transitions between the SG and PM phases described above we compare their free energies. Three cases must be distinguished

- $\beta < \beta_{\rm P}$ (but greater than the inverse of the classical critical temperature). This case is represented in Fig. 2 for $p = 3$ and $\beta = 4$. The SG and PM free energies increase monotonically with Γ. At $\Gamma = \Gamma_c$, $f_{\rm SG} = f_{\rm PM}$ and a phase transition occurs.

  As in the classical case (where the temperature is the control parameter), $m = 1$ at the transition. The spin-glass solution continues to exist beyond the transition point until $\Gamma = \Gamma_{\rm MAX} > \Gamma_c$ where it disappears. However, between Γ_c and $\Gamma_{\rm MAX}$, $m > 1$. Values of m greater than 1 do not represent physically allowed states and should not be considered. This follows from the fact that the susceptibility $\chi = \beta\,[q_d - (1-m)q_{\rm EA}]$ can be shown to be strictly *smaller* than βq_d, which implies $0 \leq m \leq 1$. Below the critical point, $f_{\rm SG} > f_{\rm PM}$ meaning that the SG solution *maximizes* the free-energy.

  The PM solution exists below the transition all the way down to $\Gamma = 0$. This solution is locally stable for all values of Γ and could be interpreted as a metastable state below Γ_c. We believe, however, that this solution should be discarded on physical grounds because it is continuosuly connected to a $\Gamma = 0$ state whose thermodynamic properties at low temperatures are unphysical: the internal energy and the susceptibility of this state diverge as $T \to 0$ whereas these quantities can be shown to be finite in the ground state of Hamiltonian (2.2). Therefore, we shall consider that the continuation of the PM solution below Γ_c is a spurious solution and that the only physically allowed phase below Γ_c in this temperature range is the SG.

The Edwards-Anderson order parameter $q_{\rm EA}$ is *discontinuous* at the transition. The transition is nevertheless of *second* order in the thermodynamic sense. This follows from the fact that $m = 1$ at Γ_c and so the effective number of degrees of freedom involved is $(1-m)q_{\rm EA} \to 0$ at Γ_c. Therefore, there is no latent heat and the linear susceptibility is continuous. However, in contrast with the SK-model, the transition is not associated with a divergence of the SG susceptibility. The situation is the same as in the replica theory of the classical model [24].

- $\beta^\star < \beta < \beta_{\rm P}$ where $T_{\rm P} - T^\star \ll T_{\rm P}$ except for very large values of p. The case $p = 10$ for $\beta = 6.5$ is represented in Fig. 3 where we show the free-energies of the two PM and the SG solutions as functions of Γ. Decreasing Γ from $\Gamma \gg 1$ we encounter two phase transitions. The first one occurs when the free energies of the two PM phases cross which signals a first order phase transition between the quantum and classical paramagnets. The glass transition occurs at a lower coupling, when the free energies of the $\rm PM_2$ and SG states cross. This transition is similar to that found for $T \geq T_{\rm P}$ and it is characterized by a discontinuity of the order parameter and the value $m = 1$ at the transition. As in the previous case, $f_{\rm SG} > f_{\rm PM_2}$ and the SG solution *maximizes* the free-energy.

- $\beta > \beta^\star$. This case is represented in Fig. 4 for $p = 3$ and $\beta = 10$. The free-energies of the states $\rm PM_1$ and $\rm PM_2$ cross as before. However, $f_{\rm SG}$ does not cross $f_{\rm PM_2}$ but it crosses $f_{\rm PM_1}$ instead. Therefore, a transition to the low-temperature ordered state can occur from $\rm PM_1$, not from $\rm PM_2$. If we were to interpret the crossings of the free energies in the standard way, we would conclude that below the transition to $\rm PM_2$ the system stays in that state down to $\Gamma = 0$. However, $\rm PM_2$, which is the continuation to low temperatures of the PM state discussed above for $\Gamma < \Gamma_c$ and $T > T_{\rm P}$, exhibits the same unphysical properties. We thus conclude that, for $\beta > \beta^\star$, the $\rm PM_1$ to $\rm PM_2$ transition is spurious and that the system stays in the $\rm PM_1$ state until the latter disappears in favor of the SG state. It should be noted that a similar situation was encountered in a study of the Ising SG model in a transverse field at low temperatures [34]. In contrast to the situation for $\beta < \beta^\star$, $f_{\rm SG} < f_{\rm PM_1}$ and the SG solution *minimizes* the free-energy. Such an inversion of the order of the free-energies was also found in a study of an anisotropic classical p-spin model [35]. It can be thought as a result of the competition between the conflicting requirement of maximization and minimization with respect to $q_{\rm EA}$ and q_d, respectively.

  We find that the break point m considered as a function of Γ has two branches. Physical values of m must be chosen from the branch that can be continued to the classical limit, $\Gamma = 0$. For $\beta > \beta^\star$, the maximum physical value of the break point $m_{\rm MAX} < 1$. The SG solution ceases to exist at the corresponding value of Γ, $\Gamma_{\rm MAX}$ (this will become more transparent in the zero temperature limit that we discuss next). An important consequence is that now m is discontinuous at the transition implying that the latter becomes *first* order. Since the physical SG and PM solutions extend beyond the point where their free-energies cross,

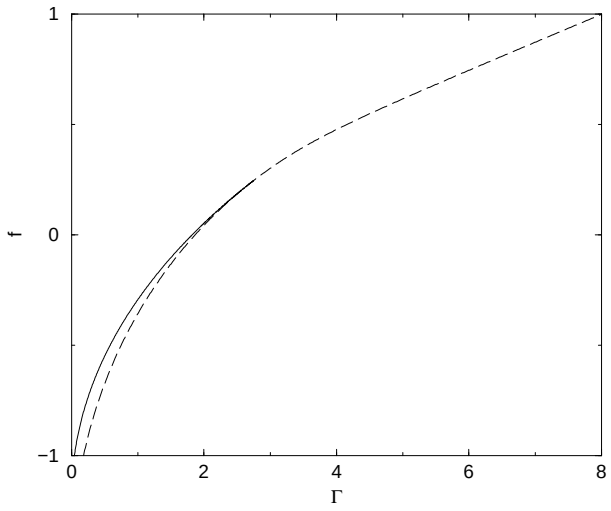

Figure 2: The SG and PM free-energies (solid and dashed lines, respectively) in the static approximation as a function of Γ for $\beta = 4$ and $p = 3$.

there is a region of phase coexistence and hysteresis is expected (see below).

The phase diagram resulting from this analysis is represented for $p = 3$ in Fig. 5 (thin lines). The PM_1 to PM_2 transition is invisible on the scale of the plot for this value of p. At low temperatures, the first order line exhibits reentrant behavior, as is the case for the Ising p-spin-glass model in a transverse field [12]. This feature is an artifact of the static approximation that disappears in the exact treatment of the problem, as we shall see in Section 4. The second and first order critical lines meet at the tricritical point $(T^\star, \Gamma^\star)$. It is interesting to notice that the 180^o rule [36] that imposes that the angle formed by the intersection of two critical lines at a tricritical point should be $< 180^o$ is satisfied in the static approximation.

3.2.3 The static approximation in the zero temperature limit

The behavior of the system can be completely elucidated at zero temperature. In this limit, the requirement that q_{EA} is finite implies

$$\beta m < +\infty \, , \tag{3.23}$$

meaning that $m \to 0$. This implies that Eq. (3.22) can be simplified to

$$\frac{p}{2}(\beta m)^2 q_d^p \;\; \sim \;\; \frac{x_p^2}{1 + x_p} \tag{3.24}$$

and $\coth(\beta\sqrt{\Gamma z}/2)$ in Eq. (3.4) can be replaced by one. The Lagrange multiplier in Eq. (3.15) becomes

$$z \sim \frac{x_p^2}{(1 + x_p) q_d \beta m} \tag{3.25}$$

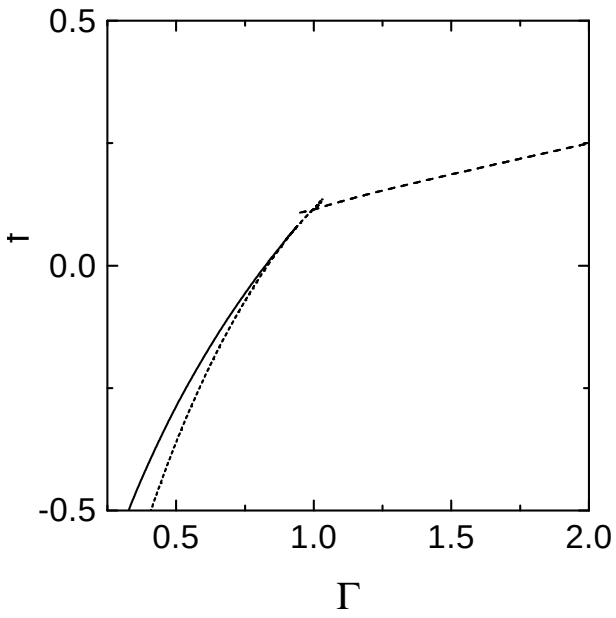

Figure 3: The SG free-energy (solid line) and the free-energies of PM_1 and PM_2 (long-dashed and dashed lines, respectively) in the static approximation as a function of Γ for $\beta = 6.5$ and $p = 10$. In this case f_{SG} intersects f_{PM_2}.

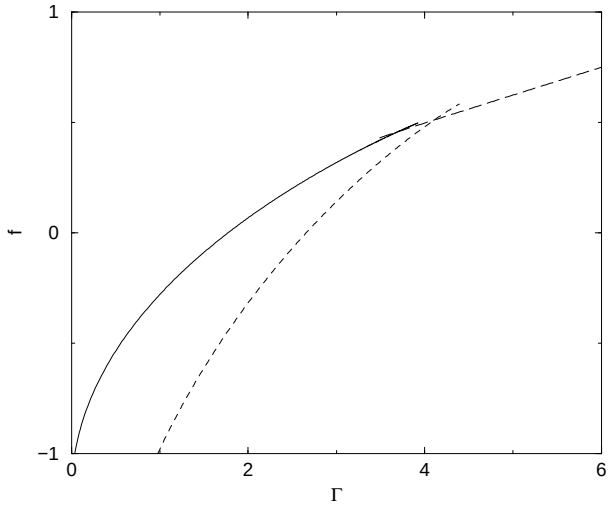

Figure 4: The SG free-energy (solid line) and the free-energies of PM_1 and PM_2 (long-dashed and dashed lines, respectively) in the static approximation as a function of Γ for $\beta = 10$ and $p = 3$. In this case f_{SG} intersects f_{PM_1}.

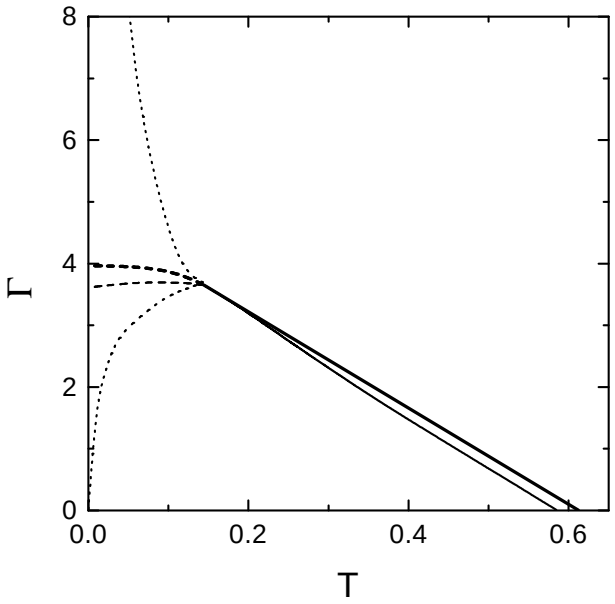

Figure 5: Static (thin lines) and dynamic (thick lines) phase diagrams of the p-spin model for $p = 3$ in the static approximation. Solid and dashed lines represent second and first order transitions, respectively. The dotted line delimits the region where two stable paramagnetic solutions coexist.

and we obtain for Γ as a function of q_d,

$$\Gamma = \sqrt{\frac{8px_p^2}{1+x_p}} q_d^{(p-2)/2} (1-q_d)^2 \ . \tag{3.26}$$

The right hand side (rhs) of this equation is a bell-shaped curve, that vanishes at $q_d = 0$ and $q_d = 1$. It reaches its maximum at $q_d^{\rm MAX} = (p-2)/(p+2)$, independently of x_p. The corresponding value of Γ is

$$\Gamma_{\rm MAX}^{\rm STATIC} = \sqrt{\frac{8px_p^2}{1+x_p}} \left(\frac{p-2}{p+2}\right)^{(p-2)/2} \left(\frac{4}{p+2}\right)^2 \ . \tag{3.27}$$

The physically meaningful solution for $\Gamma < \Gamma_{\rm MAX}^{\rm STATIC}$ must be searched on the branch corresponding to $q_d > q_d^{\rm MAX}$. This is the branch that gives the correct classical limit, $q_d = 1$ for $\Gamma = T = 0$ and has the expected property that $q_{\rm EA}$ is a decreasing function of Γ. This solution can be continued until $\Gamma = \Gamma_{\rm MAX}^{\rm STATIC}$. However, the transition occurs at a lower value Γ_c, the point at which the free-energies of the SG and $\rm PM_1$ states cross. These are respectively given by

$$f_{\rm SG} = -\frac{1}{2\beta m} \ln(1+x_p) + \frac{\sqrt{\Gamma z}}{2} + \frac{z}{2}(q_d - 1) - \frac{p\beta m}{4x_p} q_d^p - \frac{\beta m}{4} q_d^p \tag{3.28}$$

and

$$f_{\rm PM_1} = \frac{\Gamma}{8} \ . \tag{3.29}$$

At Γ_c, $q_{\rm EA}$ is finite and $m = 0$. The transition is thus of first order.

3.2.4 The condition of marginal stability in the static approximation

The condition of marginal stability leads to a different equation for the break point m. In this prescription one does not require m to be an extremum of the free-energy; instead, one requires that the replicon eigenvalue vanishes. In the static approximation, the expression derived in Section 4.4 yields:

$$\frac{1}{(q_d - q_{\rm EA})^2} - \frac{\beta^2}{2} p(p-1) q_{\rm EA}^{p-2} = 0. \tag{3.30}$$

The other extremal conditions remain unchanged. Combining Eqs. (3.16) and (3.30), and using the definitions (3.18) we arrive at

$$m = (p-2)\frac{1-y}{y} \qquad \Leftrightarrow \qquad x_p = p-2. \tag{3.31}$$

For reasons that will become apparent in Section 6, we define the *dynamic* transition line as the boundary of the region in the $T - \Gamma$ plane, with $T < T^\star$, where the marginally stable SG exists. The line $\Gamma_d(T)$ consists of two sections. The first one, that starts at the classical critical point, $(T_d, 0)$, is determined by the condition $m = 1$. The dynamic transition in this case is of the same nature as in the classical case. The condition $m = 1$ can be fulfilled until reaching a tricritical point $(T_d^\star, \Gamma_d^\star)$. At lower temperatures the marginal solution disappears before reaching the value $m = 1$.

The dynamic phase diagram for $p = 3$ is shown in Fig. 5 (thick lines). As in the equilibrium case, m is discontinuous across the dashed line. Γ_d lies always above Γ_c. According to the interpretation of this line given in Section 6, this means that the equilibrium state can never be reached dynamically starting from an initial state in the PM phase. The two lines come very close to each other for $T \sim T^\star$. Within the accuracy of our calculations we cannot assert whether they precisely touch at $T^\star$, an intriguing possibility. For $T < T^\star$, m varies continuously along $\Gamma_d(T)$ and vanishes at the quantum critical point.

It is interesting to note that the 180^o rule [36] does not hold in this out of equilibrium situation. Indeed, in Fig 5 one sees that the first order and second order line join continuously at the tricritical point.

3.2.5 The marginal stable solution in the zero temperature limit

Again in this case it is simple to obtain an analytic equation for $q_d(\Gamma)$ at zero temperature. Inserting $x_p = p - 2$ in Eq. (3.26) leads to

$$\Gamma = \sqrt{\frac{8p(p-2)^2}{p-1}} (1 - q_d)^2 q_d^{(p-2)/2} \ . \tag{3.32}$$

The maximum of this curve is also located at $q_d^{\rm MAX} = (p-2)/(p+2)$ and the physically meaningful solution is on the branch to the right of the maximum. This equation has a solution up to

$$\Gamma_{\rm MAX}^{\rm MARG} = \sqrt{\frac{8p(p-2)^2}{p-1}} \left(\frac{p-2}{p+2}\right)^{(p-2)/2} \left(\frac{4}{p+2}\right)^2 \ . \tag{3.33}$$

At zero temperature, the 1-step RSB solution with the marginal condition disappears at $\Gamma = \Gamma_{\rm MAX}^{\rm MARG}$ where m is zero.

Note that if we compare the maximum value of Γ for which there is a 1-step RSB solution with the equilibrium and marginal criteria we have

$$\Gamma_{\rm MAX}^{\rm STATIC} > \Gamma_{\rm MAX}^{\rm MARG}. \tag{3.34}$$

Hence the marginal solutions disappear at lower values of Γ than the equilibrium solutions. This result is also obtained with the quantum TAP approach [23] when one follows metastable states as functions of their energy density. This behavior is similar to that of the classical problem with varying temperature: the equilibrium solution disappears at higher temperatures than the marginal solutions [43]. This does not mean that the static transition occurs at a higher value of Γ at fixed temperature. In fact, the static transition is determined by the identity of the free-energies $f_{\rm SG} = f_{\rm PM_1}$ that at zero temperature yields $\Gamma_c^{\rm STATIC} \simeq 3.61$ and it is smaller than the dynamical critical value $\Gamma_c^{\rm DYN} \equiv \Gamma_{\rm MAX}^{\rm MARG} \simeq 3.97$.

The inequality (3.34) is valid at finite temperatures and beyond the static approximation, too. This can be checked via the full numerical solution of the problem or with the quantum TAP approach used in Ref. [23].

3.3 The simpler $p = 2$ case

The model with $p = 2$ has been studied by several authors [28, 29] and already at the classical limit it is known to show important differences with respect to the case $p \geq 3$. The transition is always second order and it is accompanied by a divergence of the SG susceptibility. There is no multiplicity of fully stable paramagnetic solutions and the spin-glass phase is RS. This statement follows from the fact that, for $p = 2$, Eq. (3.19) only admits $x_2 = 0$ as a solution. Then, Eq. (3.18) implies that, for $q_{\rm EA} \neq 0$, $m \equiv 0$. Notice that, if $p = 2$, the replicon eigenvalue (3.12) is identically zero. The RS solution is thus marginally stable, as in the classical case [39].

4 The exact solution

The static approximation neglects the imaginary-time dependence of the diagonal elements of the order-parameter matrix. In this Section we discuss the exact equations for the paramagnetic and spin-glass phases. We study the properties of the SG phase using both equilibrium and marginality conditions. In the latter case, we derive exact equations for the Edwards-Anderson parameter and the break point m that we shall later compare to the results of the real-time calculation (Section 6). We present a low-temperature and low-frequency approximation that allows us to show that the marginally stable state is the only gapless solution. It also allows us to compute the dependence of $\tilde{q}_d(0)$ on Γ, the T-dependence of the specific heat, and the low-temperature properties of $\chi(\omega \to 0)$.

4.1 Equations for the exact paramagnetic solution

In the paramagnetic phase the order parameter matrix is diagonal,

$$\tilde{Q}_{ab}(\omega_k) = \tilde{q}_d(\omega_k)\delta_{ab} \; . \tag{4.1}$$

Replacing in Eq. (2.25) we obtain the following equation for $\tilde{q}_d(\omega_k)$

$$\frac{\omega_k^2}{\Gamma} + z = \frac{1}{\tilde{q}_d(\omega_k)} + \tilde{\Sigma}(\omega_k) \; , \tag{4.2}$$

where we have defined the self-energy

$$\tilde{\Sigma}(\omega_k) \equiv \frac{p}{2}\int_0^\beta d\tau \, \exp(i\omega_k\tau)\, q_d^{p-1}(\tau) \; . \tag{4.3}$$

The Lagrange multiplier z is determined by the spherical constraint

$$q_d(0) = \frac{1}{\beta}\sum_k \tilde{q}_d(\omega_k) = 1 \; . \tag{4.4}$$

Thus, in the general case, z is determined by a non-trivial implicit equation in contrast with its analog in the static approximation, Eq. (3.8). It follows from Eq. (4.2) that the Fourier components of $q_d(\tau)$ with $k \neq 0$ are strongly suppressed in the limit $\Gamma \to 0$. The normalization condition then implies that $\lim_{\Gamma\to 0}\tilde{q}_d(\omega_k) = \beta\delta_{\omega_k,0}$ which is the classical result.

4.2 Equations for the exact spin-glass solution

The RS *Ansatz* in Fourier space is given by

$$\tilde{Q}_{ab}(\omega_k) = (\tilde{q}_d(\omega_k) - \tilde{q}_{\rm EA})\,\delta_{ab} + \tilde{q}_{\rm EA} \; . \tag{4.5}$$

The inverse matrix, $\tilde{\mathbf{Q}}^{-1}$, can be easily evaluated to yield (in the limit $n \to 0$)

$$\left(\tilde{\mathbf{Q}}^{-1}\right)_{ab}(\omega_k) = \frac{1}{\tilde{q}_d(\omega_k) - \tilde{q}_{\rm EA}}\delta_{ab} - \frac{\tilde{q}_{\rm EA}}{\left(\tilde{q}_d(\omega_k) - \tilde{q}_{\rm EA}\right)^2} \; . \tag{4.6}$$

Inserting the above expressions in Eq. (2.25) and using the identity (2.32), we get (for $a \neq b$ and $\omega_k = 0$)

$$-\frac{q_{\rm EA}}{\left(\tilde{q}_d(0) - \beta q_{\rm EA}\right)^2} + \frac{p}{2}q_{\rm EA}^{p-1} = 0 \; . \tag{4.7}$$

Note that in the classical limit $\tilde{q}_d(0) = \beta$, and one recovers the classical equation for $q_{\rm EA}$ in the RS case [24]. As in the static approximation, the replica symmetric *Ansatz* is unstable towards replica symmetry breaking. The replicon eigenvalue associated with Eq. (4.5) is

$$\Lambda_T = \frac{\beta^2}{(\tilde{q}_d(0) - \beta q_{\rm EA})^2} - \frac{\beta^2}{2}p(p-1)q_{\rm EA}^{p-2} \; . \tag{4.8}$$

This equation and Eq. (4.7) yield $\Lambda_T = p(2-p)q_{\rm EA}^{(p-2)}/2$. This eigenvalue is negative for all $p \geq 3$. This excludes a RS stable SG state and the symmetry between the replicas must be broken.

Inspired by the classical case [24], and the results from the static approximation, we use a 1-step RSB *Ansatz* that we prove to be exact in the Appendix. In Fourier space this can be written in the form

$$\tilde{Q}_{ab}(\omega_k) = (\tilde{q}_d(\omega_k) - \tilde{q}_{\rm EA})\,\delta_{ab} + (\tilde{q}_{\rm EA} - \tilde{q}_0)\,\epsilon_{ab} + \tilde{q}_0 \ , \tag{4.9}$$

where the matrix ϵ has been defined in Eq. (3.14). In the absence of an external field, the saddle point equation for q_0 yields $q_0 = 0$, as in the static approximation and the classical case [24]. The inverse matrix, $\tilde{\mathbf{Q}}^{-1}(\omega_k)$ can then be written as

$$\left(\tilde{Q}^{-1}\right)_{ab}(\omega_k) = A(\omega_k)\delta_{ab} + B(\omega_k)\epsilon_{ab} \ , \tag{4.10}$$

where (in the limit $n \to 0$)

$$A(\omega_k) = \frac{1}{\tilde{q}_d(\omega_k) - \tilde{q}_{\rm EA}} \tag{4.11}$$

and

$$B(\omega_k) = -\frac{\tilde{q}_{\rm EA}}{\tilde{q}_d^2(\omega_k) - \tilde{q}_{\rm EA}^2(m-1) + \tilde{q}_d(\omega_k)\tilde{q}_{\rm EA}(m-2)} \ . \tag{4.12}$$

The saddle point equations for $q_{\rm EA}$ and $\tilde{q}_d(\omega_k)$ can be obtained by inserting Eqs. (4.9) and (4.10) in Eq. (2.25) at $a \neq b, \omega_k = 0$ and $a = b$, respectively. They read

$$-\frac{1}{\tilde{q}_d^2(0) - \beta^2 q_{\rm EA}^2(m-1) + \beta q_{\rm EA}\tilde{q}_d(0)(m-2)} + \frac{p}{2}q_{\rm EA}^{p-2} = 0 \ , \tag{4.13}$$

and

$$\frac{\omega_k^2}{\Gamma} + z = \frac{\tilde{q}_d(\omega_k) + \beta q_{\rm EA}(m-2)\delta_{\omega_k,0}}{\tilde{q}_d^2(\omega_k) - \beta^2 q_{\rm EA}^2(m-1)\delta_{\omega_k,0} + \beta q_{\rm EA}\tilde{q}_d(\omega_k)(m-2)\delta_{\omega_k,0}} + \tilde{\Sigma}(\omega_k) \ , \tag{4.14}$$

with $\tilde{\Sigma}(\omega_k)$ defined in Eq. (4.3). Equations (4.13) and (4.14) must be supplemented by an equation for the break point parameter, m. As within the static approximation, the latter may be obtained using two different prescriptions that we discuss next.

4.3 The equilibrium spin-glass solution

In equilibrium, the free-energy per spin, f, must be stationary with respect to variations in m. The only m-dependent terms in f are

$$\frac{1}{\beta}\lim_{n\to 0}\frac{1}{n}\left(-\frac{1}{2}{\rm Tr}\ln\left(\beta^{-1}\tilde{\mathbf{Q}}(0)\right) - \frac{\beta^2}{4}n(m-1)q_{\rm EA}^p\right) \tag{4.15}$$

which can be easily evaluated with the result

$$-\frac{1}{2\beta}\left[\ln\left(\frac{\tilde{q}_d(0)-\tilde{q}_{\rm EA}(1-m)}{\beta}\right)+\frac{m-1}{m}\ln\left(\frac{\tilde{q}_d(0)-\tilde{q}_{\rm EA}}{\tilde{q}_d(0)-\tilde{q}_{\rm EA}(1-m)}\right)\right]-\frac{\beta}{4}(m-1)q_{\rm EA}^p. \tag{4.16}$$

The extremization equation $\partial f/\partial m = 0$ is

$$\frac{1}{m}\frac{\beta q_{\rm EA}}{\tilde{q}_d(0)-\beta q_{\rm EA}(1-m)}+\frac{1}{m^2}\ln\left(\frac{\tilde{q}_d(0)-\beta q_{\rm EA}}{\tilde{q}_d(0)-\beta q_{\rm EA}(1-m)}\right)+\frac{\beta^2}{2}q_{\rm EA}^p=0. \tag{4.17}$$

Combining Eqs. (4.13) and (4.17) and defining

$$y'=\frac{\beta q_{\rm EA}}{\tilde{q}_d(0)} \qquad\qquad x_p=\frac{my'}{1-y'}, \tag{4.18}$$

we obtain the same expression for x_p that we derived in the static approximation, Eq. (3.19). Using Eq. (4.13) and the definitions (4.18), we have

$$\frac{p(\beta m)^2 q_{\rm EA}^p}{2}=\frac{2x_p^2}{1+x_p} \tag{4.19}$$

and

$$\frac{p(\beta m)^2\tilde{q}_d^p(0)}{2}=\beta^p x_p^{2-p}\frac{(m+x_p)^p}{1+x_p}\ . \tag{4.20}$$

The first of these equations is identical to Eq. (3.21).

It is convenient to separate q_d and the self-energy into constant and τ-dependent parts,

$$q_d(\tau) = q_{\rm EA}+q_{\rm REG}(\tau)\ , \tag{4.21}$$

$$\Sigma(\tau) = \frac{p}{2}q_{\rm EA}^{p-1}+\Sigma_{\rm REG}(\tau)\ . \tag{4.22}$$

Substituting in Eq. (4.14) and using Eqs. (4.19) and (4.20), the terms that are proportional to $\delta_{\omega_k,0}$ cancel and we obtain an equation for the regular part of $\tilde{q_d}(\omega_k)$,

$$\frac{\omega_k^2}{\Gamma}+z'=\frac{1}{\tilde{q}_{\rm REG}(\omega_k)}+\tilde{\Sigma}_{\rm REG}(\omega_k)-\tilde{\Sigma}_{\rm REG}(0)\ , \tag{4.23}$$

where

$$z' = \frac{p}{2}\ \beta m q_{\rm EA}^{p-1}\frac{1+x_p}{x_p} \tag{4.24}$$

and

$$\tilde{\Sigma}_{\rm REG}(\omega_k)-\tilde{\Sigma}_{\rm REG}(0)=\frac{p}{2}\int_0^\beta d\tau\ (\cos(\omega_k\tau)-1)\,(q_d^{p-1}(\tau)-q_{\rm EA}^{p-1})\ . \tag{4.25}$$

4.4 The marginally stable spin-glass solution

In this Section we compute the replicon eigenvalue for the exact problem and we derive the consequences of using the condition of marginal stability that corresponds to setting it to zero.

4.4.1 The replicon eigenvalue

To derive the replicon eigenvalue, we first compute the second order variation of G_0 with respect to $\tilde{X}_{ab}(\omega_k) \equiv \tilde{Q}_{ab}(\omega_k)/\beta$ which gives the Gaussian $\tilde{\mathbf{X}}$ fluctuations:

$$\begin{aligned} 2\delta^2 G_0 &= \sum_{\omega_k} \mathrm{Tr}\left(\tilde{\mathbf{X}}^{-1}(\omega_k)\cdot\delta\tilde{\mathbf{X}}(\omega_k)\right)^2 \\ &\quad -\frac{\beta}{2}p(p-1)\sum_{ab}\sum_{\omega'_k}\sum_{\omega''_k}\int d\tau\left(\sum_{\omega_k}\exp(-i\omega_k\tau)\tilde{X}_{ab}(\omega_k)\right)^{p-2} \\ &\quad \times\exp\left[-i\tau\left(\omega'_k+\omega''_k\right)\right]\delta\tilde{X}_{ab}(\omega'_k)\delta\tilde{X}_{ab}(\omega''_k)\ . \end{aligned} \tag{4.26}$$

For the 1-step RSB *Ansatz* the eigenvalues and eigenvectors of this quadratic form may be obtained by solving the equation

$$\begin{aligned} &A^2(\omega_k)\delta\tilde{X}_{ab}(\omega_k)+A(\omega_k)B(\omega_k)\left[\left(\delta\tilde{\mathbf{X}}(\omega_k)\cdot\epsilon\right)_{ab}+\left(\epsilon\cdot\delta\tilde{\mathbf{X}}(\omega_k)\right)_{ab}\right] \\ &+B^2(\omega_k)\left(\epsilon\cdot\delta\tilde{\mathbf{X}}(\omega_k)\cdot\epsilon\right)_{ab}-\frac{p(p-1)}{2}q_{\rm EA}^{p-2}\epsilon_{ab}\delta\tilde{X}_{ab}(\omega_k)=\beta^{-2}\Lambda_T(\omega_k)\delta\tilde{X}_{ab}(\omega_k)\ , \end{aligned} \tag{4.27}$$

where $a\neq b$ and $A(\omega_k)$ and $B(\omega_k)$ are defined by Eqs. (4.11) and (4.12). Since we are looking for the replicon (transverse) eigenvalue we impose the constraints

$$\left(\epsilon\cdot\delta\tilde{\mathbf{X}}(\omega_k)\right)_{ab}=0\ , \tag{4.28}$$

$$\left(1-\epsilon_{ab}\right)\delta\tilde{X}_{ab}(\omega_k)=0\ , \tag{4.29}$$

and set $\omega_k=0$ to obtain

$$\Lambda_T=\beta^2A^2(0)-\frac{\beta^2}{2}p(p-1)q_{\rm EA}^{p-2}. \tag{4.30}$$

The condition of marginal stability corresponds to $\Lambda_T=0$ and replaces (4.17) for the determination of the break point.

4.4.2 The block-size m

Setting $\Lambda_T=0$ and using Eq. (4.13) we obtain

$$m=(p-2)\frac{\tilde{q}_d(0)-\beta q_{\rm EA}}{\beta q_{\rm EA}}=(p-2)\frac{1-y'}{y'}. \tag{4.31}$$

It follows from this expression and Eq. (4.20) that $x_p=p-2$. This is the result that we obtained in the static approximation. In the classical limit, $m=(p-$

$2)(1-q_{\rm EA})/q_{\rm EA}$, a known result [24] . Moreover, using again Eq. (4.13), the above expression can be written as

$$\beta m = (p-2)\sqrt{\frac{2}{p(p-1)}}q_{\rm EA}^{-p/2} \ , \tag{4.32}$$

which is identical to Eq. (3.21) obtained in the static approximation.

Equations (4.23)-(4.25), derived for the equilibrium state, also hold for the marginal SG provided we make the substitution $x_p \to p-2$.

4.4.3 The Edwards-Anderson order parameter

If we rewrite the denominator in the first term of Eq. (4.13) and replace m by its expression in Eq. (4.32) we obtain a new equation for $q_{\rm EA}$ that reads

$$1 = \frac{p(p-1)}{2}\left(\tilde{q}_d(0) - \beta q_{\rm EA}\right)^2 q_{\rm EA}^{p-2} = \frac{p(p-1)}{2} q_{\rm EA}^{p-2}\tilde{\chi}^2_{\rm REG}(0) \ . \tag{4.33}$$

Note the absence of explicit dependence upon Γ both here and in Eq. (4.32). The quantum parameter only enters implicitly through $\tilde{q}_d(0)$ and $q_{\rm EA}$.

An identical equation for the Edwards-Anderson parameter can also be derived with the quantum TAP approach [23] when the threshold value for the free-energy density is chosen. In the classical limit, $\tilde{q}_d(0) = \beta$ and this equation becomes the equation for $q_{\rm EA}$ of the classical TAP states of the threshold level [43].

This equation may be studied in the usual way, *i.e.*, by looking at the shape of the function that appears on its right-hand-side. This vanishes at $q_{\rm EA} = 0$ and $q_{\rm EA} = \tilde{q}_d(0)/\beta$ and has a maximum at $\beta q_{\rm EA} = \frac{p-2}{p}\tilde{q}_d(0)$. The maximum is at $m = 2$ just as in the classical problem. Two solutions for $\beta q_{\rm EA}$, one on the right-branch, the other one on the left-branch. It is simple to see that the correct physical behavior of a decreasing Edwards-Anderson parameter with increasing temperature is achieved by the solution on the right-branch.

Note, however, that other equations where $\tilde{q}_d(0)$ appears need also be satisfied in the quantum problem. These depend explicitly on the quantum parameter Γ. Depending on Γ and T the marginally stable SG may disappear before reaching the $m = 2$ value.

4.4.4 The low-frequency limit

The existence of a vanishing transverse eigenvalue implies that the spectrum of magnetic excitations of the marginally stable SG state is gapless. Therefore, at $T = 0$, $q_{\rm REG}(\tau)$ is expected to decay asymptotically as a power-law:

$$q_{\rm REG}(\tau) \sim \frac{A}{|\tau|^\alpha} \qquad |\tau| \to \infty \ . \tag{4.34}$$

Equivalently, the imaginary part of the susceptibility $\chi''(\omega)$ vanishes as $\omega^{(\alpha-1)}$ as $\omega \to 0$. In the zero temperature limit the Matsubara frequencies are continuous and

Eq. (4.25) becomes

$$\tilde{\Sigma}_{\rm REG}(\omega) - \tilde{\Sigma}_{\rm REG}(0) = \frac{p}{2}\int_{-\infty}^{\infty} d\tau \ (\cos\omega\tau - 1)\left[(p-1)q_{\rm EA}^{p-2} q_{\rm REG}(\tau) + \ldots\right] . \quad (4.35)$$

The terms represented by the dots contain higher powers of $q_{\rm REG}(\tau)$. In the $\omega \to 0$ the integral is dominated by the long τ limit, and we may replace $q_{\rm REG}(\tau)$ by its asymptotic form (4.34). Eq. (4.35) becomes

$$\tilde{\Sigma}_{\rm REG}(\omega) - \tilde{\Sigma}_{\rm REG}(0) \approx \frac{p(p-1)}{2} A q_{\rm EA}^{p-2} \int_{-\infty}^{\infty} d\tau \ \frac{\cos(\omega\tau) - 1}{|\tau|^{\alpha}} , \quad (4.36)$$

leading to

$$\tilde{\Sigma}_{\rm REG}(\omega) - \tilde{\Sigma}_{\rm REG}(0) \approx p(p-1) A q_{\rm EA}^{p-2} \Gamma[1-\alpha] \ \sin\left(\frac{\alpha\pi}{2}\right) \ |\omega|^{\alpha-1} , \quad (4.37)$$

where $\Gamma[x]$ is the Gamma function. The higher order terms neglected in Eq. (4.35) give rise to terms vanishing as higher powers of ω. Likewise,

$$\tilde{q}_{\rm REG}(\omega) - \tilde{q}_{\rm REG}(0) \approx 2A\Gamma[1-\alpha] \ \sin\left(\frac{\alpha\pi}{2}\right) \ |\omega|^{\alpha-1} . \quad (4.38)$$

Replacing Eqs. (4.37) and (4.38) in Eq. (4.23) and comparing terms of order $|\omega|^{\alpha-1}$ we obtain

$$z' = \frac{p(p-1)}{2} \, q_{\rm EA}^{p-1} \beta \frac{1-y'}{y'} , \quad (4.39)$$

which compared with Eq. (4.24) gives

$$x_p = p - 2 , \quad (4.40)$$

the marginal value of x_p. We thus see that the marginally stable state is the only one compatible with a gapless spectrum. Conversely, the equilibrium state must necessarily have a gap in its excitation spectrum.

In order to determine the values of the exponent α and the amplitude A, we proceed by keeping only the first term on the rhs of Eq. (4.35),

$$\tilde{\Sigma}_{\rm REG}(\omega_k) - \tilde{\Sigma}_{\rm REG}(0) \approx \frac{p(p-1)}{2} q_{\rm EA}^{p-2} \left(\tilde{q}_{\rm REG}(\omega_k) - \tilde{q}_{\rm REG}(0)\right) , \quad (4.41)$$

and replace it in Eq. (4.23) noting that $\tilde{q}_{\rm REG}(0) = \tilde{q}_d(0) - \beta q_{\rm EA} \equiv \beta m q_{\rm EA}/(p-2)$ (cf. Eqs. (4.18) and (4.40)). The result is

$$\left[\frac{\omega_k^2}{\Gamma} + \frac{p(p-1)}{p-2}\beta m q_{\rm EA}^{p-1} - \frac{p(p-1)}{2} q_{\rm EA}^{p-2} \tilde{q}_{\rm REG}(\omega_k)\right] \tilde{q}_{\rm REG}(\omega_k) = 1 . \quad (4.42)$$

The solution of this quadratic equation is

$$\tilde{q}_{\rm REG}(\omega_k) = \frac{\frac{\omega_k^2}{\Gamma} + \frac{p(p-1)}{p-2}\beta m q_{\rm EA}^{p-1} - |\omega_k| \, \Gamma^{-1/2} \sqrt{\frac{\omega_k^2}{\Gamma} + \frac{2p(p-1)}{p-2}\beta m q_{\rm EA}^{p-1}}}{p(p-1) q_{\rm EA}^{p-2}} . \quad (4.43)$$

This result is only valid in the limit $\omega_k \to 0$ where it reduces to

$$\tilde{q}_{\rm REG}(\omega_k) \sim \tilde{q}_d(0) - \beta q_{\rm EA} - \frac{(\tilde{q}_d(0) - \beta q_{\rm EA})^{1/2} q_{\rm EA}^{1-p/2} \sqrt{2/[p(p-1)]}}{\sqrt{\Gamma}} \, |\omega_k| \qquad (4.44)$$

Thus, the exponent giving the asymptotic decay of $q_d(\tau)$ in Eq. (4.34) is $\alpha = 2$. Substituting Eqs. (4.19), (4.20) and (4.40) in Eq. (4.44) and analytically continuing to real frequencies we obtain the exact result

$$\lim_{\omega \to 0} \frac{\chi''(\omega)}{\omega} = \frac{1}{\sqrt{\Gamma}} \left[\frac{2\, q_{\rm EA}^{(2-p)}}{p(p-1)} \right]^{3/4} \quad . \qquad (4.45)$$

One can easily show that the amplitude A is obtained by multiplying the rhs of the equation above by π.

It is interesting to notice that a linear excitation spectrum has also been found in the case of the SU($\mathcal{N}$) Heisenberg SG model [32]. However, in our model this gapless spectrum is not a consequence of Goldstone's theorem as the model does not possess any continuous symmetry.

4.4.5 An approximate solution of the dynamical equations

The results of the previous section suggest a simple approximate solution of the complete set of equations that becomes exact in the low-frequency and low-temperature limit. Once $\tilde{q_d}(\omega)$ is known, the equation of state, $q_{\rm EA}(T, \Gamma)$, must be determined from the normalization condition

$$1 - q_{\rm EA} = \frac{1}{\beta} \sum_{\omega_k} \tilde{q}_{\rm REG}(\omega_k) \equiv \int_0^\infty \frac{d\omega}{\pi} \chi''(\omega) \coth(\beta\, \omega/2) \ . \qquad (4.46)$$

If we assume that the integral is dominated by the low frequencies, we can compute it by replacing $\chi''(\omega)$ by the analytic continuation of Eq. (4.43). The result at $T = 0$ is

$$1 - q_{\rm EA} = \frac{4}{3\pi} \frac{\sqrt{\Gamma}}{\left[p(p-1) q_{\rm EA}^{p-2}/2 \right]^{1/4}} \ , \qquad (4.47)$$

which reduces to

$$\Gamma = \left(\frac{3\pi}{4} \right)^2 \left[p(p-1) q_{\rm EA}^{p-2}/2 \right]^{1/2} (1 - q_{\rm EA})^2. \qquad (4.48)$$

This equation has the same form as the corresponding one obtained with the static approximation, Eq. (3.33); only the coefficient is different. For $p = 3$, we find that the maximum coupling for the marginal SG state, that is also the critical coupling at zero temperature, is $\Gamma_d(0) = 2.75$ compared to $\Gamma_d(0)$=3.97 in the static approximation and the estimate $\Gamma_d(0) = 3.1$ from the numerical calculations to be described below. It is easy to check that, at finite but low temperature, the corrections to Eq. (4.47) are of $\mathcal{O}(T^2)$. Therefore,

$$q_{\rm EA}(T, \Gamma) = q_{\rm EA}(0, \Gamma) \left[1 - \mathcal{O}(T^2) \right] \ , \qquad (4.49)$$

as $T \to 0$.

We shall compare quantitatively the low-frequency approximation with the numerical solution of the exact equations in Section 5.

4.5 Thermodynamic functions

The free-energy per spin may be calculated by substituting our *Ansatz* for the order-parameter matrix in Eqs. (2.23) and (2.24). After some algebra we obtain:

$$\begin{aligned}
\beta f &= -\frac{1}{2}\left\{\log\left[1-(1-m)y'\right] + \frac{m-1}{m}\log\frac{1-y'}{1-(1-m)y'}\right\} \\
&- \frac{\beta^2}{4}(m-1)q^p_{\rm EA} - \frac{\beta}{4}\int_0^\beta d\tau q^p_d(\tau) - \frac{\beta z}{2} + \ln\left[2\sinh\left(\beta\sqrt{\Gamma z}/2\right)\right] \\
&- \frac{1}{2}\sum_\omega \ln\left[\left(\frac{\omega^2}{\Gamma}+z\right)\tilde{q}_d(\omega)\right] + \frac{1}{2}\sum_\omega\left[\left(\frac{\omega^2}{\Gamma}+z\right)\tilde{q}_d(\omega) - 1\right].
\end{aligned} \tag{4.50}$$

The entropy, internal energy and specific heat are given by

$$S = -\frac{\partial f}{\partial T}\,, \qquad U = \frac{\partial(\beta f)}{\partial \beta}\,, \qquad C_v = \frac{\partial U}{\partial T}\,, \tag{4.51}$$

respectively.

The derivatives needed to compute S and U must be taken only with respect to the *explicit* T-dependence of the free-energy. Contributions from terms of the form $\partial(\beta f)/\partial q_{\rm EA} \times \partial q_{\rm EA}/\partial T$ and alike vanish because of the stationarity condition. A convenient way to proceed consists in observing that $q_d(\tau)$ is a dimensionless function and, as such, it can only depend on dimensionless variables. We can choose them as follows

$$q_d(\tau, \tilde{J}, \Gamma, T) = \hat{q}_d(\tau/\beta, \beta z, \beta\tilde{J}, \Gamma/\tilde{J})\,. \tag{4.52}$$

It follows that

$$U_2 \equiv -\frac{\beta}{4}\int_0^\beta d\tau q^p_d(\tau) = -\frac{\beta^2}{4}\int_0^1 ds\ \hat{q}^p_d(s, \beta z, \beta\tilde{J}, \Gamma/\tilde{J})\,, \tag{4.53}$$

and its explicit derivative with respect to β is

$$\frac{\partial U_2}{\partial \beta} = -\frac{\beta}{2}\int_0^1 ds \hat{q}^p_d(s, \beta z, \beta\tilde{J}, \Gamma/\tilde{J}) = -\frac{1}{2}\int_0^\beta d\tau q^p_d(\tau)\,. \tag{4.54}$$

Similarly,

$$\tilde{q}_d(\omega_k) = \int_0^\beta d\tau q_d(\tau) e^{i\omega_k\tau} = \beta\int_0^1 ds \hat{q}_d(s) e^{i2\pi k s} \equiv \beta\hat{q}_d(k). \tag{4.55}$$

The explicit β dependence of $\tilde{q}_d(\omega)$ is thus a multiplicative factor. Finally, we observe that $\partial\omega_k/\partial\beta = -\omega_k/\beta$. Using these considerations, we derived the following expression for the internal energy:

$$U = -\frac{\beta}{2}(m-1)q^p_{\rm EA} - \frac{1}{2}\int_0^\beta d\tau q^p_d(\tau) + \frac{z}{2} + \frac{1}{2\beta}\sum_{\omega_k}\left[1 - \left(\frac{\omega_k^2}{\Gamma}+z\right)\tilde{q}_d(\omega_k)\right]. \tag{4.56}$$

We analyze separately the PM and SG phases.

4.5.1 Internal energy of the paramagnetic phase

The equation of motion can be recast as

$$1 - \left(\frac{\omega_k^2}{\Gamma} + z \right) \tilde{q}_d(\omega_k) = -\tilde{\Sigma}(\omega_k) \tilde{q}_d(\omega_k) \; ; \tag{4.57}$$

replacing this expression in the last term of Eq. (4.56) and using

$$\frac{1}{\beta} \sum_{\omega_k} \Sigma(\omega_k) \tilde{q}_d(\omega_n) \equiv \int_0^\beta d\tau \; \Sigma(\tau) q_d(\tau) = \frac{p}{2} \int_0^\beta d\tau \; q_d^p(\tau) \; , \tag{4.58}$$

we obtain a very simple expression for the paramagnetic internal energy:

$$U_{\rm PM} = \frac{z}{2} - \frac{p+2}{4} \int_0^\beta d\tau \; q_d^p(\tau) \; . \tag{4.59}$$

Since we have shown that a gapless spectrum is only possible in the marginally stable SG state, there must be a gap $E_{\rm G}$ in the spectrum of the paramagnetic phase. Therefore the specific heat in the PM phase vanishes exponentially at low temperature:

$$C_v \propto \exp(-E_{\rm G}/T) \; . \tag{4.60}$$

4.5.2 Internal energy in the spin-glass phase

The same procedure can be applied to the SG phase, using this time the equation of motion in the form

$$\left[\frac{\omega_k^2}{\Gamma} + z - \tilde{\Sigma}(\omega_k) \right] \tilde{q}_d(\omega_k) = 1 + (f_p - 1) \delta_{\omega_k, 0} \; , \tag{4.61}$$

where

$$f_p = 1 + \frac{x_p^2}{m(1+x_p)} - \frac{x_p^2}{m^2(1+x_p)} \; . \tag{4.62}$$

By substituting Eq. (4.61) into Eq. (4.56) we obtain

$$U_{\rm SG} = \frac{z}{2} - \frac{p+2}{4} \beta m \, q_{\rm EA}^p - \frac{p+2}{4} \int_0^\beta d\tau \, (q_d^p(\tau) - q_{\rm EA}^p) \; , \tag{4.63}$$

where βm is given by Eq. (4.19) and z

$$z = \frac{p}{2} \beta m \, q_{\rm EA}^{p-1} \, \frac{1+x_p}{x_p} + \tilde{\Sigma}_{\rm REG}(\omega = 0) \; , \tag{4.64}$$

and

$$\tilde{\Sigma}_{\rm REG}(\omega = 0) = \frac{p}{2} \int_0^\beta d\tau \left(q_d^{p-1}(\tau) - q_{\rm EA}^{p-1} \right) \; . \tag{4.65}$$

In the equilibrium SG state the specific heat vanishes exponentially as its excitation spectrum has a gap.

Since f is not an extremum with respect to m in the marginal state, it would seem that the term $\partial(\beta f)/\partial m \times \partial m/\partial T$ should appear in the calculation of its internal energy. However, it can be shown that in the correct expression of the energy density of this state, that coincides with the one obtained in the real-time dynamics calculation, such contributions are absent. Hence, we shall use Eq. (4.56) also in the marginal case. Since now $q_{\rm REG}(\tau) \equiv q_d(\tau) - q_{\rm EA} \sim \tau^{-1}$ at $T = 0$, we expect C_v to have a power-law dependence upon T. Indeed, since at low temperature the integral in Eq. (4.63) is dominated by the long-time behavior of $q_d(\tau)$, we can evaluate the latter by Fourier transforming Eq. (4.43). The resulting expression depends on T only through $q_{\rm EA}$. It follows from Eq. (4.49) that, in the marginal SG state, $C_v \propto T$. This power-law behavior is reminiscent of the temperature dependence of low-temperature glasses that has been intensively studied experimentally [17].

5 Numerical solution

In this Section we present numerical solutions obtained using an algorithm that solves the equations of Section 4. All the results reported in this Section where obtained for $p = 3$.

5.1 The paramagnetic phase

The PM phase is described by Eq. (4.2) subject to the spherical constraint (2.27). At each temperature, the equations are solved iteratively as a function of Γ, starting from high and low values of this parameter. In these limits we can find analytical perturbative solutions that are used as starting points for the iteration procedure. For each value of Γ, the input is the converged solution obtained for the previous value.

For $\beta < \beta_{\rm P} \approx 6$, Eq. (4.2) has only one solution that is connected continuously to both the high and low-Γ limits. Fig. 6(a) shows the function $q_d(\tau)$ for $\beta = 4$ and several values of Γ. The correlation function in imaginary time decreases monotonically as a function of τ in the interval $[0, \beta/2]$. The initial slope increases with Γ. For large Γ the decay is exponential, reflecting the presence of a well developed gap in the excitation spectrum. Fig. 6(b) represents the Γ-dependence of the free-energy per spin for the same value of β. For $\Gamma \gg 1$, it approaches a T-independent asymptote, $f = \Gamma/8$.

For $\beta > \beta_{\rm P}$, the solutions obtained for $\Gamma \gg 1$ and $\Gamma \ll 1$ are still unique but they are not continuously connected. The solution that derives from that for $\Gamma \gg 1$ ($\rm PM_1$) can only be followed down to a critical coupling $\Gamma = \Gamma_{c2}$, where it ceases to exist. Conversely, the solution that exists for $\Gamma \ll 1$ ($\rm PM_2$) can be followed only up to $\Gamma = \Gamma_{c1}$. Since $\Gamma_{c2} < \Gamma_{c1}$ the two solutions coexist in the interval $\Gamma_{c2} \leq \Gamma \leq \Gamma_{c1}$. Figure 7 shows the two types of solutions for $\beta = 8$ and several values of Γ. For this temperature, the two paramagnets coexist in the region $2.8 \leq \Gamma \leq 3.6$. The corresponding free-energies are shown in Fig. 7 (b). The free-energies cross at a point intermediate between Γ_{c2} and Γ_{c1}. Notice that, below the crossing point, the

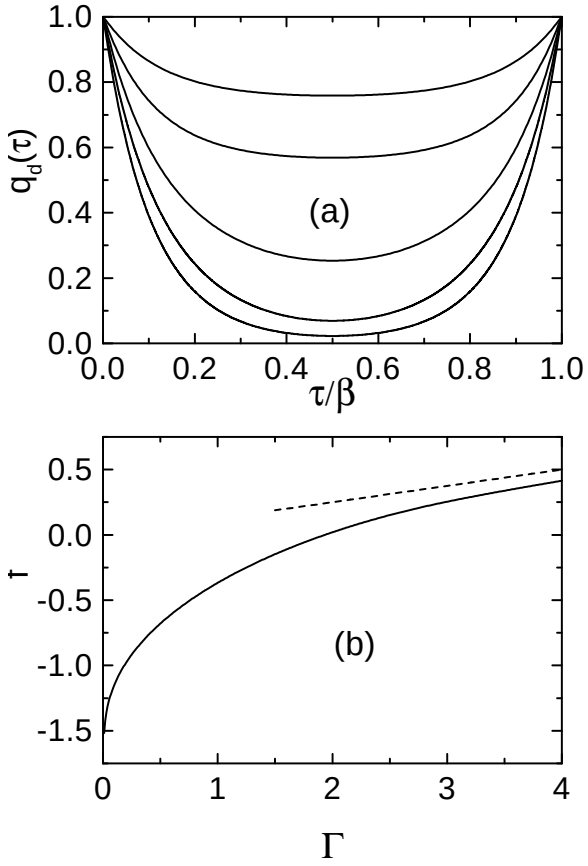

Figure 6: (a) The function $q_d(\tau)$ for the PM solution at $\beta = 4$ and $\Gamma = 1, 2, 3, 4, 5$ from top to bottom. (b) The PM free-energy as a function of Γ at $\beta = 4$. The dashed line is the asymptotic value $f = \Gamma/8$.

classical PM has the lowest free-energy. These results are reminiscent of those found within the static approximation with PM_1 and PM_2 corresponding to the solutions with $q_d = q_d^<$ and $q_d = q_d^>$ of Section 3, respectively.

The two PM states are qualitatively different. In the quantum PM, $q_d(\tau)$ decreases exponentially in $0 \leq \tau \leq \beta/2$. In the classical PM, after a transient, $q_d(\tau)$ levels-off to a τ-independent value that decreases with increasing Γ. An analysis of the connection between $q_d(\tau)$ and $\chi''(\omega)$ given in Eq. (2.30) allows us to understand these differences in terms of the spectral properties of the two states. We find that the exponential decay of the correlation function of the quantum paramagnet reflects the presence of a gap in $\chi''(\omega)$ and that the plateau that appears in the case of the classical paramagnet reveals the presence of a central peak with a narrow width $\Delta\omega \ll T$ in the gap. The hight of the plateau measures the fraction of the total spectral weight under the peak.

5.2 The spin-glass phase

The equations that describe the SG phase contain an extra parameter, the break point m. The solutions are found as follows. Fixing β and m, we compute q_{EA}, $\tilde{q}_d(0)$

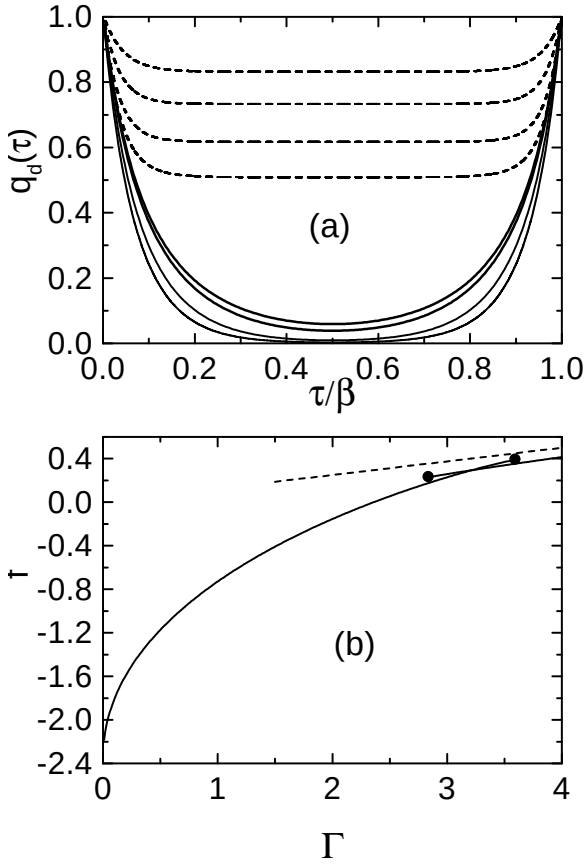

Figure 7: (a) $q_d(\tau)$ for the PM solutions at $\beta = 8$. Solid lines: classical PM solutions. $\Gamma = 1, 2, 3, 3.5$ from top to bottom. Dashed lines: quantum PM solutions. $\Gamma = 2.8, 3, 3.5, 4$ from top to bottom. (b) Solid Lines: free-energies of PM solutions as functions of Γ at $\beta = 8$. The solid circles are the points at $\Gamma_{c1} = 3.6$ and $\Gamma_{c2} = 2.8$ where the solutions cease to exist. Dashed line: the asymptotic value $f = \Gamma/8$.

and z' from Eqs. (4.19), (4.20) and (4.24), respectively. The value of x_p is chosen according to whether we want to study the equilibrium or the marginal SG states. We then solve Eq. (4.23) iteratively varying Γ, starting from $\Gamma = 0$, until a value is found that satisfies the spherical constraint. For each temperature lower than the classical transition temperature, this procedure is repeated for different values of m.

This procedure allows us to determine a function $m \equiv m(T, \Gamma)$. As shown in Fig. 8 for $\beta = 20$, $m(T, \Gamma)$ has two branches that meet at $\Gamma = \Gamma_{\max}(T)$. Physical values of m lie on the branch that satisfies that $m(T, \Gamma = 0) = m_{\text{CLASS}}(T)$, the classical break point. There are no solutions of Eq. (4.23) for $\Gamma > \Gamma_{\max}(T)$ which may be identified as the value of the coupling above which quantum fluctuations destroy the SG phase.

We found that, as in the static approximation, there exists a temperature $T^\star$ such that, for $\beta \geq \beta^\star$, $m_{\max}(T) < 1$. In all cases q_{EA} is finite at $\Gamma_{\max}(T)$. This fact and Eq. (4.19) imply that $\lim_{T\to 0} m_{\max}(T) = 0$, meaning that replica symmetry is restored at the quantum critical point. The same feature was previously found in a

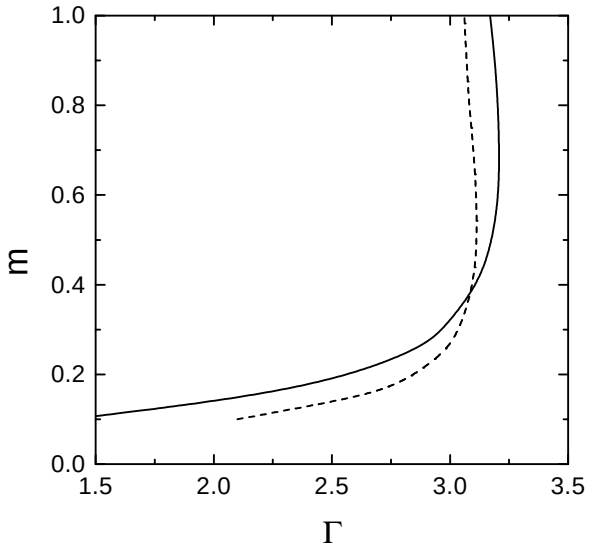

Figure 8: The breaking point m as a function of Γ for $p = 3$ and $\beta = 20$, both for the equilibrium (solid line) and marginally stable (dashed line) SG state. For the equilibrium state $(\Gamma_{\rm MAX}, m_{\rm MAX}) \simeq (3.21, 0.7)$. For the marginally stable SG state $(\Gamma_{\rm MAX}, m_{\rm MAX}) \simeq (3.12, 0.5)$.

study of the SU($\mathcal{N}$) Heisenberg model [32].

Fig. 9 shows the regular part of the auto-correlation function (cf. Eq. (4.21)), for $\beta = 4$ and $\beta = 12$ and values of Γ in the SG phase. It may be seen that $q_{\rm REG}(\tau)$ decays more rapidly in the equilibrium state than in the marginally stable state. Analysis of the curves of Fig. 9 for $\beta = 12$ shows that, for $1 \ll \tau \ll \beta/2$, $q_{\rm REG}(\tau)$ decays exponentially in the first case but $q_{\rm REG}(\tau) \propto \tau^{-2}$ in the second one. This follows again from the differences in the excitation spectra of the two states.

In the case of the marginally stable solution, $q_{\rm REG}(\tau)$ may also be computed using the low-frequency approximation of Section 4.4.5. The exact and approximate results for $\beta = 20$ are shown in Fig. 10. It can be seen that the agreement between the two is very good.

5.3 Equilibrium phase diagram

In this section we discuss the phase diagram that results from the analysis of the equilibrium solutions. The case of the marginally stable solutions will be discussed in the next Section. As within the static approximation, all the PM states that we found are locally stable. Their free-energies must be compared with that of the SG state in order to construct the equilibrium phase diagram. As before, there exists a temperature interval $T^\star \leq T \leq T_{\rm P}$ within which there are two first order transitions as a function of Γ, one from the quantum to the classical PM, followed at a lower coupling by the SG transition. However, for $p = 3$, the case for which we have performed detailed numerical calculations, $T_{\rm P} - T^\star$ is very small and, in the following, we only consider in detail the cases $T > T_{\rm P}$ and $T < T^\star$. Figures 11(a) and (b) show the Γ-dependence of the PM and SG free-energies for $p = 3$ computed

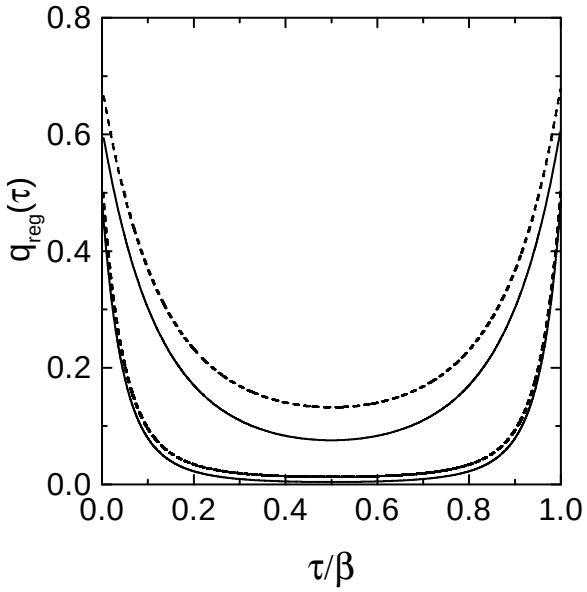

Figure 9: Regular part of the auto-correlation function in the SG phase. Full and dashed lines represent the equilibrium and marginally stable states, respectively. Upper curves: $\beta = 4$, $\Gamma = 2.35$. Lower curves: $\beta = 12$, $\Gamma = 1.75$.

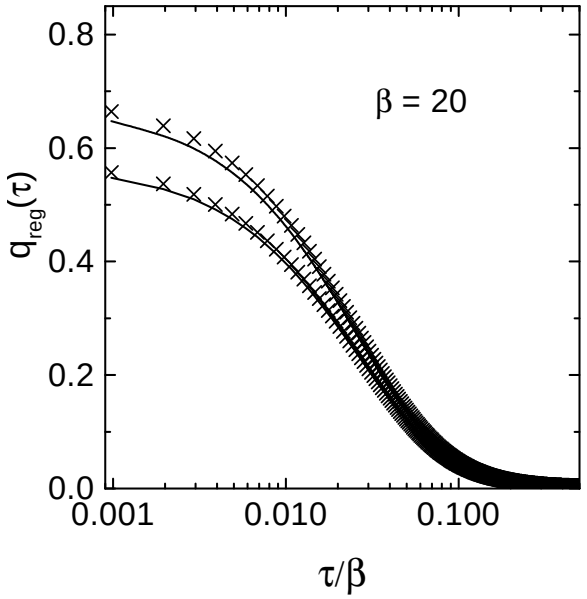

Figure 10: Comparison of the exact numerical solution for $q_{\rm REG}(\tau)$ (solid lines) and the approximation of Section 4.4.5 (symbols) for $\beta = 20$. Upper curves: $\Gamma = 2.0$. Lower curves $\Gamma = 3.0$.

using Eq. (2.24) for two temperatures, above $T_{\rm P}$ and below $T^\star$. Solid lines and symbols represent the PM and SG solutions, respectively. The curves end at the point where the corresponding solution disappears. It may be seen that for $T > T_{\rm P}$ the free-energies of the two states merge precisely at $\Gamma_c(T)$ where $m = 1$. Below the critical point, $f_{\rm SG} > f_{\rm PM}$ meaning that the SG solution *maximizes* the free-energy. As in the static approximation, stability arguments do not exclude the PM solution below Γ_c as a metastable state but we may resort to the arguments given in Section 3 to argue that the continuation of the PM solution into the SG phase is unphysical also in this case.

Below $T^\star$ we must compare the free-energies of the two PM solutions with that of the SG state to choose the most favorable phase. In this temperature range, the classical paramagnet has the same unphysical properties that we found in Section 3 in the static approximation: the ground-state energy and susceptibility diverge and its free energy does not intersect that of the ordered state. Therefore, we discard it in favor of $\rm PM_1$ even if its free-energy is higher. The free-energies of the SG and $\rm PM_1$ states cross at $\Gamma_c < \Gamma_{\rm max}$ as shown in the inset in Fig. 11(b). As in the static approximation, $f_{\rm SG} < f_{\rm PM}$ for $T < T^\star$ whereas $f_{\rm SG} > f_{\rm PM}$ for $T > T^\star$. The SG and $\rm PM_1$ solutions extend beyond the point where their free-energies cross and there is phase coexistence. Now, both $q_{\rm EA}$ and m are discontinuous at Γ_c. The SG transition is thus *first* order with latent heat and discontinuous susceptibility (see below). The phase diagram resulting from this analysis is represented in Fig. 12 (thin lines). The flat section is the first-order line, which *does not* exhibit the spurious reentrant behavior found within the static approximation (Fig. 5). In addition, in contrast with the approximate phase diagram, the transition line has zero-slope at $T = 0$, which is a consequence of the third law of thermodynamics as shown in Ref. [12].

We also computed the Γ-dependence of $q_{\rm EA}$ and the static susceptibility,

$$\chi = \int_0^\beta d\tau \, [q_d(\tau) - (1-m) q_{\rm EA}] \, , \tag{5.1}$$

as functions of Γ for the $p = 3$ model. The results are displayed in Fig. 13. The susceptibility has a cusp at Γ_c for $T > T^\star$ and a discontinuity for $T < T^\star$. The dotted lines correspond to the regions of metastability. Notice that the susceptibility is *higher* on the SG side of the transition, an unusual result. This follows from the fact that the gap in the excitation spectrum of the PM state is wider than that of the SG state. For the same reason the entropy of the PM is *lower* leading to a *negative* latent heat at the transition.

As shown in the lower pannel of Fig. 13, the order parameter decreases rapidly with increasing Γ and is reduced by a factor of two half-way from the transition, showing that quantum fluctuations are quite strong in this system.

As mentioned above, early experiments [1] on $\rm LiHo_xY_{1-x}F_4$ in a transverse magnetic field suggested that the second order SG transition observed for moderate fields could become first order for $H \approx H_c(0)$, the field above which the system remains PM down to zero temperature. The recent observation of hysteresis effects in the transverse field-dependence of the susceptibility give further support to this idea [5]. While the model that we study here is not intended to describe microscopically this

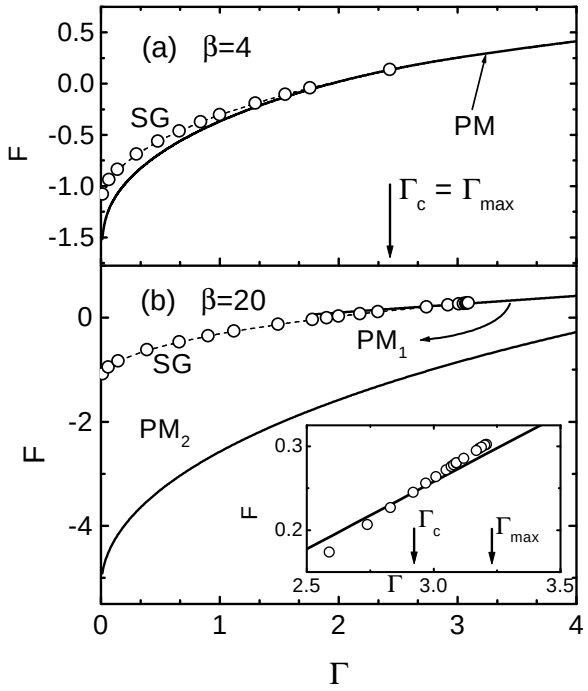

Figure 11: Free-energies of the different PM (solid lines) and SG (symbols) phases above $T_{\rm P}$ (a) and below $T^\star$ (b). The inset in panel (b) shows in detail the crossing of the free-energies at the critical point for $T < T^\star$.

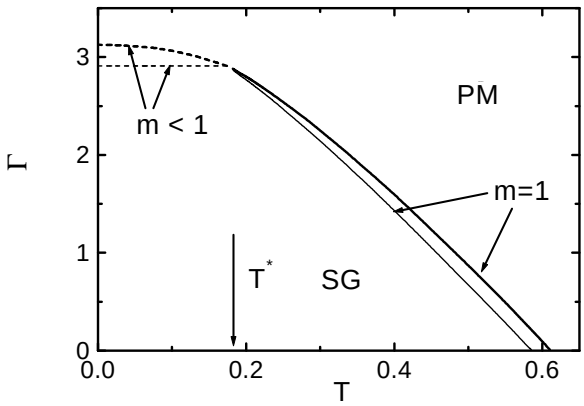

Figure 12: Static (thin lines) and dynamic (thick lines) phase diagrams of the p-spin model for $p = 3$. Solid and dashed lines represent second and first order transitions, respectively.

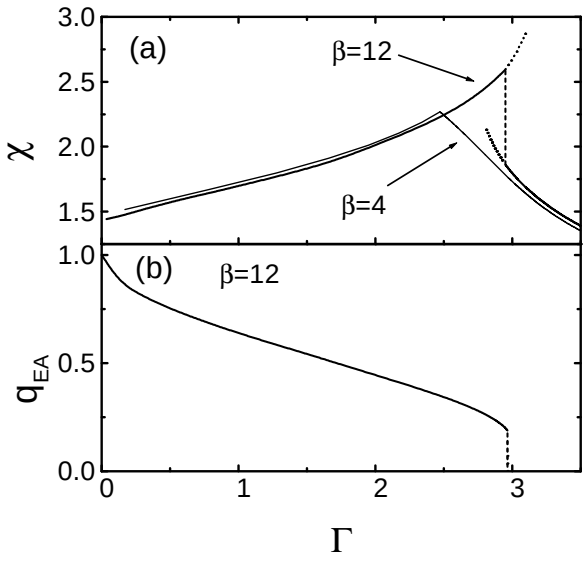

Figure 13: Magnetic susceptibility (a) and Edwards-Anderson order parameter (b) of the p=3 model.

compound, it captures some of its phenomenology. However, important differences between the predictions of this model and experiment exist, the most important ones being the fact that, in the model, where the transition is second order, it *is not* accompanied by a divergence of χ_3 and that the jump of χ across the first order transition line has a sign opposite to that observed experimentally.

6 Connections between the marginally stable state and real time dynamics

As is well known, the dynamics of *classical* spin-glasses becomes non-stationary below a dynamic transition temperature T_d that may or may not coincide with T_g. In the low-temperature phase, the systems shows *aging*, *i.e.*, the correlation function $C(t, t')$ depends both on the time-difference $(t - t')$ and on t' [40, 41, 42]. Aging has experimental manifestations such as a dependence of the ac-susceptibility on frequency and the time elapsed after a quench. Theoretical studies of aging effects in quantum systems have recently appeared in the literature [20, 44, 45, 46]. Some systems where quantum fluctuations might play a role, like magnetic nanoparticles [47] and disordered $2D$-electronic systems [48], were investigated experimentally. A search for these effects in the Li(Ho/Y)F_4 system is under way [5].

The existence of connections between dynamic and static calculations in classical disordered systems is known since the work of Sompolinsky on the equilibrium dynamics of the SK model [49]. Apart from some conceptual problems that have been extensively discussed in the literature [50], Sompolinsky noted that his dynamic solution for the classical SK model was marginally stable. Kirkpatrick and Thirumalai [51] showed that, in the classical mean-field p-spin-glass model, T_d can

be calculated in a fully static replica approach if the break point m is computed by demanding that the spin-glass susceptibility $\chi_{\rm SG}$ diverges, instead of asking that the free-energy be an extremum with respect to variations of this parameter. In technical terms, this prescription corresponds to setting the replicon eigenvalue to zero [52] and goes under the name of *condition of marginal stability*. It has already been used within the Matsubara approach to quantum disordered problems on the basis of the physical assumptions of having a gapless solution [53, 32].

In this Section we compare the results obtained above using the marginal stability criterion with the outcome of a full dynamical calculation of the same system *weakly* coupled to a quantum bath made of an ensemble of harmonic oscillators [20]. The Hamiltonian of the coupled system is

$$H = H_{\rm SYST} + H_{\rm BATH} + \alpha H_{\rm INT} \ , \tag{6.1}$$

with $H_{\rm SYST}$ given in (2.2). $H_{\rm BATH}$ is the Hamiltonian of an ensemble of quantum harmonic oscillators with an Ohmic spectral density. $H_{\rm INT}$ represents a linear coupling between the spins and the oscillators' displacements and it is controlled by a coupling constant α. The oscillators are in equilibrium at temperature T at all times and act as a reservoir.

The real-time evolution of the system was derived using the Schwinger-Keldysh formalism and it is described by coupled differential equations for $C(t,t')$ and $R(t,t')$, the symmetrized correlation and response functions of the system, respectively [20]. In the glassy phase, C exhibits a two-time dependence of the form:

$$C(t+t_w,t_w) = C_{\rm ST}(t) + C_{\rm AG}(t+t_w,t_w) \ . \tag{6.2}$$

The first term gives the time-dependent evolution for time-differences $t \ll t_w$ and varies between $1-q_{\rm EA}$ to 0. In this time regime, the second term is constant and equal to $q_{\rm EA}$ but decays from $q_{\rm EA}$ to 0 in a waiting-time dependent manner when $t \gg t_w$. More formally, the Edwards-Anderson parameter is defined as

$$q_{\rm EA} \equiv \lim_{t\to\infty} \lim_{t_w\to\infty} C(t+t_w,t_w) \ . \tag{6.3}$$

The response function can also be written by separating two terms as in (6.2)

$$R(t+t_w,t_w) = R_{\rm ST}(t) + R_{\rm AG}(t+t_w,t_w) \ . \tag{6.4}$$

The first term is invariant under time-translations and it is related to the first term in (6.2) by the quantum fluctuation-dissipation theorem (FDT). The second term is related to the second term in (6.2) by a modified quantum FDT relation where the temperature of the bath T is replaced by an effective temperature $T_{\rm EFF} \equiv T/X$ which defines X, the FDT violation factor [21]. In the long-t_w limit,

$$R_{\rm AG}(t+t_w,t_w) = \frac{X}{T} \left. \frac{\partial C_{\rm AG}(t+t_w,t')}{\partial t'} \right|_{t'=t_w} \ . \tag{6.5}$$

For the model under consideration, weakly coupled to a bath, the FDT violation factor and $q_{\rm EA}$ are given by [20]

$$\beta X = \frac{p-2}{q_{\rm EA}} R_{\rm ST}(\omega=0) \equiv (p-2)\sqrt{\frac{2}{p(p-1)}} q_{\rm EA}^{-p/2} \,, \tag{6.6}$$

$$1 = \frac{p(p-2)}{2} q_{\rm EA}^{p-2} R_{\rm ST}^2(\omega=0) \,. \tag{6.7}$$

These equations have the same form as Eqs. (4.32) and (4.33) with m and $\tilde{q}_{\rm REG}(0)$ replaced by X and $R_{\rm ST}(\omega=0)$, respectively. It will be shown below that, in the limit $\alpha \to 0$, the equation obeyed by $R_{\rm ST}(\omega)$ reduces to the analytic continuation of Eq. (4.23). Therefore, in this limit, $R_{\rm ST}(\omega=0) = \tilde{q}_{\rm REG}(i\omega_k=0)$. It follows from this fact and Eqs. (4.32)-(4.33) and (6.6)-(6.7) that $m = X$. Although the coincidence between the values of X and m for the marginal SG state has been noticed several times for classical models, this is the first explicit evidence of its validity in a quantum problem.

This correspondence allows us to identify the dynamic transition line $\Gamma_d(T)$ as the boundary in the $T-\Gamma$ plane where the marginally stable solution exists. $\Gamma_d(T)$ is a piecewise curve formed by a line on which $X=1$ that joins $(T_d,0)$ and $(T^\star,\Gamma^\star)$ and a line on which $X<1$ that joins $(T^\star,\Gamma^\star)$ and $(0,\Gamma_c)$. The dynamic phase diagram for $p=3$ is shown in Fig. 12 (thick lines). It is qualitatively similar to that obtained in the static approximation. In particular, m is discontinuous across the dashed line and Γ_d lies always above Γ_c. Notice that the two transition lines come very close to one another for $T \sim T^\star$ and seem to touch at $T^\star$. For $T < T^\star$, m varies continuously along $\Gamma_{\rm d}(T)$ and vanishes at the quantum critical point[55]. This has a consequence of potential interest for experiment: at low temperatures, FDT violations are predicted to appear suddenly as $\Gamma_{\rm d}$ is crossed coming from the high Γ region.

The equivalence between the replica theory supplemented with the marginality condition (RTMC) and the dynamical approach goes beyond the equality of m and X. It also holds for the expectation values of operators calculated within RTMC and the long-time limit of the same observables in the coupled dynamical system, for $\alpha \to 0$. It must be stressed that the weak-coupling limit must be taken *after* the thermodynamic and long-time limits [54]. More precisely, one can establish that for an operator O depending only on the coordinates and momenta of the system,

$$\langle O \rangle_{\rm RTMC} = \lim_{\alpha\to 0} \lim_{t\to\infty} \lim_{N\to\infty} \langle O(t) \rangle_{\rm DYN} \,, \tag{6.8}$$

where $\langle \cdots \rangle_{\rm RTMC}$ is the outcome of the RTMC calculation.

To illustrate this point, we consider Eq. (4.23) fixing $p=3$ for simplicity. We define the real-time quantities

$$\begin{aligned} &\tilde{R}_{\rm RTMC}(\omega) = \tilde{q}_{\rm REG}(i\omega_k)\big|_{i\omega_k\to\omega+i0^+} \;, \quad R_{\rm RTMC}(t) = \textstyle\int_{-\infty}^{\infty} \frac{d\omega}{2\pi}\, \tilde{R}_{\rm RTMC}(\omega) \exp(-i\omega t) \,, \\ &\tilde{\Sigma}_{\rm RTMC}(\omega) = \tilde{\Sigma}_{\rm REG}(i\omega_k)\Big|_{i\omega_k\to\omega+i0^+} \;, \quad \Sigma_{\rm RTMC}(t) = \textstyle\int_{-\infty}^{\infty} \frac{d\omega}{2\pi}\, \tilde{\Sigma}_{\rm RTMC}(\omega) \exp(-i\omega t) \,, \end{aligned} \tag{6.9}$$

and introduce the Lehmann representations

$$\tilde{q}_{\rm REG}(i\omega_k) = \int_{-\infty}^{\infty} \frac{d\omega}{\pi} \frac{{\rm Im}\, \tilde{R}_{\rm RTMC}(\omega)}{\omega - i\omega_k} \,, \qquad \tilde{\Sigma}_{\rm REG}(i\omega_k) = \int_{-\infty}^{\infty} \frac{d\omega}{\pi} \frac{{\rm Im}\, \tilde{\Sigma}_{\rm RTMC}(\omega)}{\omega - i\omega_k} \,. \tag{6.10}$$

It follows from Eqs. (6.9) and (6.10) that

$$\begin{aligned} R_{\rm RTMC}(t) &= \theta(t) \int_{-\infty}^{\infty} \tfrac{d\omega}{\pi}\ {\rm Im}\, \tilde{R}_{\rm RTMC}(\omega) \sin(\omega t)\ , \\ \Sigma_{\rm REG}(t) &= \theta(t) \int_{-\infty}^{\infty} \tfrac{d\omega}{\pi}\ {\rm Im}\, \tilde{\Sigma}_{\rm RTMC}(\omega) \sin(\omega t)\ . \end{aligned} \tag{6.11}$$

Analytically continuing Eq. (4.23) and Fourier transforming the resulting equation we arrive at

$$\left[\frac{1}{\Gamma}\,\frac{\partial^2}{\partial t^2} + z_{\rm RTMC}\right] R_{\rm RTMC}(t) = \delta(t) + \int_0^t dt'\ \Sigma_{\rm RTMC}(t-t') R_{\rm RTMC}(t')\ , \tag{6.12}$$

where the limits on the integral on the right-hand side follow from Eq. (6.11) and

$$z_{\rm RTMC} = z' + \tilde{\Sigma}_{\rm REG(0)} \equiv R^{-1}_{\rm RTMC}(\omega = 0) + \int_0^{\infty} dt'\ \Sigma_{\rm RTMC}(t'). \tag{6.13}$$

The last equality follows from the combined use of Eqs. (4.24), Eqs. (4.19) and (4.33). Rewriting Eq. (4.25) for $p = 3$ in the form

$$\tilde{\Sigma}_{\rm REG}(i\omega_k) = \frac{3}{2\beta} \sum_{\omega_m} \tilde{q}_{\rm REG}(i\omega_m)\ \tilde{q}_{\rm REG}(i\omega_k - i\omega_m) + 3 q_{\rm EA}\ \tilde{q}_{\rm REG}(i\omega_k)\ , \tag{6.14}$$

and using Eq. (6.10), we find after some algebra

$${\rm Im}\ \Sigma_{\rm RTMC}(\omega) = \frac{3}{2} \int_{-\infty}^{\infty} \frac{d\omega'}{\pi} C_{\rm RTMC}(\omega')\ {\rm Im}\ R_{\rm RTMC}(\omega' - \omega)\ , \tag{6.15}$$

where we have introduced the Fourier transform of the symmetrized correlation function

$$C_{\rm RTMC}(\omega) = {\rm Im}\ R_{\rm RTMC}(\omega)\ \coth \frac{\beta\omega}{2} + 2\pi\ q_{\rm EA}\ \delta(\omega). \tag{6.16}$$

It follows that

$$\Sigma_{\rm RTMC}(t) = 3\ \theta(t) C_{\rm RTMC}(t)\ R_{\rm RTMC}(t) \equiv -3\ {\rm Im} \left[C_{\rm RTMC}(t) - \frac{i}{2} R_{\rm RTMC}(t)\right]^2\ . \tag{6.17}$$

Equations (6.12), (6.13) and (6.17) are equivalent to Eqs. (6.6), (6.16), (7.13) and (3.27) of Ref. [20] specialized to $p = 3$ and taken in the limit $\alpha \to 0$. It follows that

$$R_{\rm RTMC}(t) = \lim_{\alpha\to 0} \lim_{t_w \to \infty} R_{\rm DYN}(t + t_w, t_w) = \lim_{\alpha \to 0} R_{\rm ST}(t)\ . \tag{6.18}$$

The equality of the RTMC response function and the stationary part of the dynamical response function implies that all the quantities that can be expressed in terms of them are also equal. In particular, it can be shown that the asymptotic dynamic energy-density of the system in contact with the bath in the weak coupling limit is precisely given by Eq. (4.63).

7 Conclusions and discussion

In this paper we presented a detailed study of the properties of the quantum spherical p-spin-glass model in thermodynamic equilibrium and in the marginally stable state.

We solved the equations that describe the different phases of the system numerically and also using various approximation schemes that give valuable physical insights, in particular, on the delicate issue of handling the multiplicity of solutions of the equations.

We established explicitly a connection between the states obtained in the quantum replica calculation with the marginality condition and those that result form the non-equilibrium dynamics of the system weakly coupled to an environment in thermal equilibrium.

We determined the phase diagram of the model and showed that, in all cases, quantum fluctuations drive the SG transition first-order at sufficiently low temperatures. A tricritical point separates the two transition lines. This shows that the properties of SG systems in the quantum regime can be qualitatively different from those in the classical limit. The same feature has been first observed in the $p \to \infty$ limit of the p-spin model in a transverse field [11] and in a quantum model with multiple interactions studied in Ref. [12]. These studies, as well as the TAP analysis of Ref. [23], suggest that this phenomenon may be rather generic in quantum extensions of models having a *discontinuous* transition in the classical limit.

We notice, however, that Ritort studied the phase transition in the random orthogonal model (ROM) [56] in a transverse field within the static approximation and found no evidence of the existence of a tricritical point [57]. In this case, an expansion of the free-energy in powers of $m - 1$ leads to a vanishing Edwards-Anderson parameter at the quantum critical point $(0, \Gamma_c)$ [58]. It would be interesting to investigate whether this behavior subsists beyond the static approximation, *i.e.* whether a tricritical point at finite temperature appears in the exact solution.

A quantum particle (or a manifold) in an infinite dimensional random potential has a discontinuous classical transition when the potential has short-range correlations [62]. Therefore, the quantum extensions analyzed by Goldschmidt [63] and Giamarchi and Le Doussal [53] are hence candidates to exhibit a first order transition in the limit of zero temperature.

So far, studies of quantized models with *continuous* classical transitions have found continuous transitions close to the quantum critical point. However, we believe that this issue should be explored further. Full solutions of the low-temperature phase of these models do not yet exist. They would need a full replica symmetry breaking *Ansatz* for the non-diagonal terms in the replica matrix. In our opinion the soft spin quantum model whose real-time dynamics has been studied by Kennett and Chamon [46] is the simplest choice to investigate this question.

Many of the results of this paper can also be obtained using the TAP approach [23]. This formalism, that avoids the use of replicas, allows us to understand the organization of the metastable states and to interpret the dynamic behavior of glassy systems in terms of them. The relationship between the quantum TAP equations and the Matsubara approach for this model was analyzed In Ref. [23]. A

relationship between $(q_{\rm EQ}, m, q_d(\tau))$ in the replica approach and $(q_{\rm EQ}, \mathcal{E}, C(\tau))$ in the TAP approach was obtained where $\mathcal{E}$ is the energy density of a TAP solution and $C(\tau)$ the imaginary-time dependent correlation function. Different choices for m, such as the equilibrium condition the marginality condition or others, correspond to different choices for $\mathcal{E}$: the equilibrium value, the value reached dynamically or some intermediate one, respectively.

In Section 2.2 we mentioned that this model can be viewed as a description of a closed polymer embedded in an infinite dimensional space with a random potential [25, 26, 27]. The line tension favors a linear configuration of the polymer while the disorder makes the polymer wander and search for configurations that are favorable from an energetic point of view. As seen above, besides a transition line separating a liquid-like phase from a glassy-like phase, we expect a transition line between two different liquid phases corresponding to the two paramagnetic solutions that we found in the spin-glass model. One of the liquid phases is characterized by a large value of the correlation of two monomers separated at maximum distance $L/2$, with L the total length of the polymer. (In the static approximation we called this solution $q_d^>$.) In the polymer language, the other solution corresponds to a state in which the correlation of two monomers at distance $L/2$ is small and close to zero at high values of Γ. These two configurations can be interpreted as representing a coiled polymer ($q_d^>$) and a linear-like polymer ($q_d^<$). These results seem reasonable since the solution $q_d^<$ appears at high values of Γ, *i.e.* when the polymer is very flexible, while the solution $q_d^>$ appears at low values of Γ when the polymer is more rigid. The nature of the transition from the liquid-like to the glassy-like phase is different in the two situations. This transition is expected to occur on a sizable region of phase space only for $p \gg 1$ which corresponds to short range correlations of the random potential. It would be interesting to check whether such a crossover occurs in finite dimensional models of random directed polymers and in experiments.

This work can be extended in several directions. One of them is the question of how the choice of particular initial conditions affect the real-time dynamics of these disordered quantum models. Up to now, only the case of random initial conditions, which simulate an instantaneous quench from the high-temperature phase, was discussed in the literature [20]. An interesting problem is the relaxation dynamics within metastable states that are solutions of the quantum TAP equations [23], in the manner of Refs. [50] and [59]. To solve this problem one has to represent the generating functional of the correlation functions in the form of a path integral on a time contour that mixes real and imaginary times. The derivation of the relevant equations and their solution are not straightforward and need, as input, the solution of the imaginary-time equilibrium equations studied in this paper. We shall discuss this problem elsewhere [60]. Another open problem is how the coupling to a strong quantum environment modifies the statics and dynamics of such disordered models, an issue that we shall discuss in a separate publication [61].

8 Acknowledgements

Useful discussions with G. Biroli, T. Garel, A. Georges, J. Kurchan, L. B. Ioffe, G. Lozano, D. Mukamel, O. Parcollet, F. Ritort, M. Rozenberg and V. R. Vieira are gratefully acknowledged. We thank particularly G. Aeppli and T. Rosenbaum for making their results available to us prior to publication. LFC and DRG thank the ECOS-Sud programme for a travel grant. LFC acknowledges financial support from the ACI "Algorithmes d'optimisation et systèmes désordonnés quantiques". CAdSS is financially supported by the Portuguese Research Council, FCT, under grant PRAXIS XXI/BPD/16303/98.

Appendix

In this appendix, we demonstrate that, for the model studied in this paper, the extremization equations for a 2-step RSB *Ansatz* collapse into the ones for the 1-step RSB. This procedure can be iterated for a k-step RSB in order to prove that the 1-step RSB scheme is exact.

Within a k-step RSB *Ansatz*, the n replicas are organized into n/m_1 "1-families" of m_1 elements each. The m_1 replicas in a "1-family" are then further organized into m_1/m_2 "2-families" of m_2 elements each, and so on until the level of "k-families" is reached. We use the convention that all replicas belong to the same "0-family" so that $m_0 = n$ and $m_{k+1} = 1$. Off diagonal elements of a k-step RSB matrix Q_{ab} for which a and b belong to the same "l-family" are labeled q_l. A 2-step RSB matrix $\mathbf{Q}$ is then characterized (at zero magnetic field, that is, $q_0 = 0$) by two off-diagonal elements, q_1 and q_2, and two break points, m_1 and m_2, such that, in the $n \to 0$ limit, $0 \leq m_1 \leq m_2 \leq 1$. The only terms in the free-energy density that depend on these parameters are given by

$$-\frac{1}{2\beta}\left[\log(\tilde{q}_d(0)/\beta - \langle\langle q\rangle\rangle) + \frac{1}{m_1}\log\left(1 + m_1\frac{q_1}{\tilde{q}_d(0)/\beta - \langle\langle q\rangle\rangle}\right) + \frac{m_2-1}{m_2}\log\left(\frac{\tilde{q}_d(0)/\beta - q_2}{\tilde{q}_d(0)/\beta - \langle\langle q\rangle\rangle}\right)\right] - \frac{\beta}{4}(m_2-1)q_2^p - \frac{\beta}{4}(m_1-m_2)q_1^p\,, \qquad \text{(A.1)}$$

where $\langle\langle q\rangle\rangle = q_2 + m_2(q_1 - q_2)$. Hence, the extremization equations in order to q_1, q_2, m_1 and m_2 are given by

$$-\frac{q_1}{[\tilde{q}_d(0) + (m_2-1)\beta q_2 + (m_1-m_2)\beta q_1](\tilde{q}_d(0) - \beta\langle\langle q\rangle\rangle)} + \frac{p}{2}q_1^{p-1} = 0\,, \qquad \text{(A.2)}$$

$$\left[1 - \frac{\beta q_1}{(\tilde{q}_d(0) + (m_2-1)\beta q_2 + (m_1-m_2)\beta q_1)} + \frac{\beta q_1 - \tilde{q}_d(0)}{\tilde{q}_d(0) - \beta q_2}\right] \times\frac{\beta}{\tilde{q}_d(0) - \beta\langle\langle q\rangle\rangle} + \frac{p}{2}\beta^2 q_2^{p-1} = 0\,, \qquad \text{(A.3)}$$

$$\frac{1}{m_1^2}\log\left(\frac{\tilde{q}_d(0)-\beta\langle\langle q\rangle\rangle}{\tilde{q}_d(0)-(1-m_2)\beta q_2+(m_1-m_2)\beta q_1}\right)+\frac{\beta^2}{2}q_1^p + \frac{1}{m_1}\frac{\beta q_1}{\tilde{q}_d(0)-(1-m_2)\beta q_2+(m_1-m_2)\beta q_1}=0 \tag{A.4}$$

and

$$\frac{1}{m_2^2}\log\left(\frac{\tilde{q}_d(0)-\beta\langle\langle q\rangle\rangle}{\tilde{q}_d(0)-\beta q_2}\right)+\frac{\beta^2}{2}(q_1^p-q_2^p) + \frac{q_1-q_2}{\tilde{q}_d(0)-\beta\langle\langle q\rangle\rangle}\left(\frac{\beta^2 q_1}{\tilde{q}_d(0)-\beta\langle\langle q\rangle\rangle+m_1\beta q_1}+\frac{\beta}{m_2}\right)=0\,, \tag{A.5}$$

respectively. As can be easily seen, for $q_1=q_2$ and $m_1=m_2$ (or $m_2=1$), the above set of equations yield the 1-step result. In order to demonstrate that the 1-step solution is unique, we now compute the linear combinations $-p\times$ Eq. (A.4)$+\beta^2 q_1\times$ Eq. (A.2) and $\beta^2 q_1\times$ Eq. (A.2) $-q_2\times$ Eq. (A.3) $-p\times$ Eq. (A.5) and define $x_p=(\beta q_1)/\tilde{q}_d(0)$ and $y=(\beta q_2)/\tilde{q}_d(0)$, to obtain the following equations:

$$\begin{aligned} & \frac{x_p^2}{(1+(m_2-1)y_p+(m_1-m_2)x_p)(1-y_p-m_2(x_p-y_p))} \\ + \;& \frac{1}{m_1}\frac{px_p}{1+(m_2-1)y_p+(m_1-m_2)x_p} \\ - \;& \frac{p}{m_1^2}\log\left(\frac{1+(m_2-1)y_p+(m_1-m_2)x_p}{1-y_p-m_2(x_p-y_p)}\right)=0 \end{aligned} \tag{A.6}$$

and

$$\frac{x_p-y_p}{1-y_p-m_2(x_p-y_p)}\left[\frac{x_p(p+1)}{1+(m_2-1)y_p+(m_1-m_2)x_p}+\frac{y_p}{1-y_p}+\frac{p}{m_2}\right] + \frac{p}{m_2^2}\log\left(\frac{1-y_p-m_2(x_p-y_p)}{1-y_p}\right)=0, \tag{A.7}$$

respectively. At this point, it is useful to define the parameters

$$u_p=\frac{m_2(x_p-y_p)}{1-y_p} \tag{A.8}$$

and

$$v_p=\frac{m_1 x_p}{1-y_p} \tag{A.9}$$

and rewrite eqs. (A.7) and (A.7) as

$$\frac{v_p^2}{(1-u_p+v_p)(1-u_p)}+\frac{v_p p}{1-u_p+v_p}-p\log\left(1+\frac{v_p}{1-u_p}\right)=0 \tag{A.10}$$

and

$$\left(\frac{m_2}{m_1}\frac{v_p(1+p)}{1-u_p+v_p}-u_p+\frac{m_2}{m_1}v_p+p\right)\frac{u_p}{1-u_p}-p\log\left(\frac{1}{1-u_p}\right)=0, \tag{A.11}$$

respectively. The only real solution to the above equations is $u_p=0$ and v_p equals its 1-step value (for example, $v_p=1.81696$ for $p=3$). Therefore, we can conclude that the 2-step RSB scheme yields back the 1-step one.

References

[1] W. Wu, B. Ellmann, T. F. Rosenbaum, G. Aeppli and D. H. Reich, Phys. Rev. Lett. **67** 2076 (1991); W. Wu, D. Bitko, T. F. Rosenbaum and G. Aeppli, Phys. Rev. Lett. **71** 1919 (1993); J. Brooke, D. Bitko, T. F. Rosenbaum and G. Aeppli, Science **284**, 779 (1999).

[2] M. A. Kastner, R. J. Birgenau, G. Shirane ane Y. Endoh, Rev. Mod. Phys. **70**, 987 (1998).

[3] R. Vollmer, T. Pietrus and H. V. Löneysen, Phys. Rev. B **61**, 1218 (2000).

[4] E. Courtens, J. Phys. Lett. (Paris) **43** L199 (1982), Phys. Rev. Lett. **52** 69 (1984). E. Matsushita and T. Matsubara Prog. Theor. Phys. **71** 235 (1984). R. Pirc, B. Tadic and R. Blinc, Z. Phys. **B61** 69 (1985), Phys. Rev. **B36** 8607 (1987).

[5] G. Aeppli and T. F. Rosenbaum (private communication).

[6] D. S. Fisher, Phys. Rev. Lett. **69**, 534 (1992); Phys. Rev. **B51**, 6411 (1995). H. Rieger and A. P. Young, *Quantum Spin-glasses* (Springer-Verlag, Berlin, 1996), cond-mat/9607005. R. N. Bhatt, *Quantum spin-glasses*, in "Spin-glasses and random fields', A. P. Young ed. (World Scientific, Singapore, 1997). F. Igloi and H. Rieger, Phys. Rev. Lett. **78** 2473 (1997), H. Rieger and F. Igloi, Europhys. Lett. **39** 135 (1997).

[7] A. Bray and M. A. Moore, J. Phys. C **13**, L655 (1980).

[8] J. Miller and D. A. Huse, Phys. Rev. Lett. **70**, 3147 (1993). H. Ishii and T. Yamamoto, J. Phys. **C18**, 6225 (1985). T. Yamamoto and H. Ishii, J. Phys. **C20**, 6053 (1987).

[9] D. R. Grempel and M. Rozenberg, Phys. Rev. Lett. **80**, 389 (1998). M. Rozenberg and D. R. Grempel, Phys. Rev. Lett., **81**, 2550, (1998).

[10] S. Sachdev, N. Read and R. Oppermann, Phys. Rev. B **52**, 10 286 (1995). N. Read, S. Sachdev and J. Ye, Phys. Rev. B **52**, 384 (1995). A. M. Sengupta and A. Georges, Phys. Rev. B **52**, 10 295 (1995). D. R. Grempel and M. J. Rozenberg, Phys. Rev. B60, 4702 (1999).

[11] Y. Y. Goldschmidt, Phys. Rev. **B41** 4858 (1990).

[12] T. M. Nieuwenhuizen and F. Ritort, Physica **A250**, 89 (1998).

[13] S. K. Ghattak and D. Sherrington, J. Phys. **C10**, 3149 (1977). P. J. Mottishaw and D. Sherrington, J. Phys. **C18**, 5201 (1985). P. J. Mottishaw, Europhys. Lett. **1**, 409 (1986).

[14] H. Feldmann and R. Oppermann, J. Phys. **A33**, 1325 (2000) and references therein. This model is indeed equivalent to the classical Ghattak-Sherrington model.

[15] L. F. Cugliandolo, D. R. Grempel and C.A. da Silva Santos, Phys. Rev. Lett.**85**, 2589, (2000).

[16] R. Zeller and R. Pohl, Phys. Rev. **B4**, 2029 (1971).

[17] S. Rogge, D. Natelson and D. D. Osheroff, Phys. Rev. Lett. **76**, 3136 (1996). S. Rogge, D. Natelson, B. Tigner and D. D. Osheroff, Phys. Tev. **B55**, 11256 (1997). D. Natelson, D. Rosenberg and D. D. Osheroff, Phys. Rev. Lett. **80**, 4689 (1998).

[18] P. W. Anderson, B. Halperin and C. Varma, Phil. Mag. **25**, 1 (1972); W. Phillips, J. Low Temp. Phys. **7**, 351 (1972).

[19] H. Lozza, Master thesis, Universidad Nacional de Buenos Aires, Argentina. L. F. Cugliandolo, D. R. Grempel, G. Lozano and H. Lozza, unpublished.

[20] L. F. Cugliandolo and G. Lozano, Phys. Rev. Lett. **80** 4979 (1998), Phys. Rev. **B59**, 915 (1999).

[21] L. F. Cugliandolo, J. Kurchan and L. Peliti, Phys. Rev. **E55**, 3898 (1997).

[22] More precisely,this connection allows us to determine how the real-time correlation function $C(t,t')$ approaches its plateau value $q_{\rm EA}$ for $(t-t') \ll t'$ but not how it decays below $q_{\rm EA}$ for $(t-t') \gg t'$.

[23] G. Biroli and L. F. Cugliandolo, *Quantum TAP equations*, cond-mat/0011028.

[24] A. Crisanti and H-J Sommers, Z. Phys. **B87** 341 (1992).

[25] T. Halpin-Healy and Y-C Zhang, Phys. Rep. **254**, 215 (1995).

[26] A. Maumgartner and M. Muthukumar in Advances in chemical physics (vol XCIV), I. Prigogine and S. A. Rice eds. (J. Wiley & sons, New York, 1996).

[27] Y. Shiferaw and Y. Y. Goldschmidt, cond-mat/0003136 and references therein.

[28] P. Shukla and S. Singh, Phys. Lett. **A81**, 477 (1981). T. Vojta, Phys. Rev. **B53**, 710 (1996). T. Vojta and M. Schreiber, Phys. Rev. **53**, 8211 (1996).

[29] S. Sachdev and Y. Ye, Phys. Rev. Lett. **70**, 3339 (1993). N. Read, S. Sachdev and Y. Ye, Phys. Rev. **B52**, 384 (1995).

[30] V. Dobrosavljevic and D. Thirumalai, J. Phys. **A22** L767 (1990). L. De Cesare, K. Lubierska-Walasek, I. Rabuffo and K. Walasek, J. Phys. **A29** 1605 (1996). T. Kopeć, Phys. Rev. **B52**, 9590 (1995).

[31] T. M. Nieuwenhuizen, Phys. Rev. Lett. **74**, 4293 (1995); *ibid*, 4289 (1995).

[32] A. Georges, O. Parcollet and S. Sachdev, Phys. Rev. Lett., **85**, 840 (2000) and cond-mat/9909239.

[33] R. P. Feynmann and A. R. Hibbs, *Quantum mechanics and path integrals*, McGraw-Hill, New York, 1965.

[34] M. J. Rozenberg and D. R. Grempel, unpublished.

[35] P. J. Mottishaw, Europhys. Lett. **1**, 409 (1986).

[36] J. Wheeler, J. Chem. Phys. **C7**, 1671 (1974). We thank David Mukamel for attracting our attention to this reference.

[37] D. M. Kagan, L. B. Ioffe and M. V. Feigel'man; Sov Phys JETP **116**, 1450 (1999).

[38] P. Chandra, L. B. Ioffe and D. S. Sherrington, Phys. Rev. Lett. **75**, 713 (1995). P. Chandra, M. V. Feigel'man and L. B. Ioffe, Phys. Rev. Lett. **76**, 4805 (1996). P. Chandra, M. V. Feigel'man, L. B. Ioffe and D. M. Kagan, Phys. Rev. **B56**, 11553 (1997).

[39] J. M. Kosterlitz, D. J. Thouless and R. C. Jones, Phys. Rev. Lett. **36**, 1217 (1976).

[40] D. S. Fisher and D. Huse, Phys. Rev. **B38**, 386 (1988).

[41] J-P Bouchaud, J. Phys. I (France) **2**, 1705 (1992). J-P Bouchaud and D. S. Dean, J. Phys. I (France) **5**, 265 (1995).

[42] L. F. Cugliandolo and J. Kurchan, Phys. Rev. Lett. **71**, 173 (1993).

[43] J. Kurchan, G. Parisi and M. A. Virasoro, J. Phys. (France) I **3**, 1819 (1993).

[44] A. Mauger and N. Potier, cond-mat/9912028, cond-mat/0004068.

[45] F. Igloi and H. Rieger, cond-mat/0003193.

[46] M. P. Kennett and C. Chamon, cond-mat/0009099.

[47] R. Sappey, E. Vincent, M. Ocio, J. Hammann, J. Magn. Magn. Mat. **177**, 957 (1998). R. Sappey, E. Vincent, N. Hadacek, F. Chaput, J.P. Boilot, D. Zins, Phys. Rev. **B56**, 14551 (1997). T. Jonsson, J. Mattsson, C. Djurberg, F. A. Kahn, P. Nordblad and P. Svedlindh, Phys. Rev. Lett. **75**, 4138 (1995). T. Jonsson, J. Mattsson, P. Nordblad, P. Svedlindh, J. Magn. Magn. Mat. **168**, 269 (1997).

[48] A. Vaknin, Z. Ovadyahu, M. Pollak, Phys. Rev. Lett. 84, 3402 (2000).

[49] H. Sompolinsky, Phys. Rev. Lett. **47**, 935 (1981).

[50] A. Houghton, S. Jain and A. P. Young, Phys. Rev. **28**, 2630 (1983).

[51] T. R. Kirkpatrick and D. Thirumalai, Phys. Rev. Lett. **58**, 2091 (1987); Phys. Rev. **B36**, 5388 (1987).

[52] A. J. Bray and M. A. Moore, J. Phys. **C12**, L441 (1979).

[53] T. Giamarchi and P. Le Doussal, Phys. Rev. **B53** 15206 (1996).

[54] H. G. Schuster and V. R. Vieira, Phys. Rev. **B34**, 189 (1986).

[55] In Ref. [20] a discontinuous transition with $X = 1$ all along the critical line was *assumed* and scaling laws for the critical behaviour derived on that basis. The results of this paper show that this assumption is not applicable to the model.

[56] E. Marinari, G. Parisi and F. Ritort, J. Phys. **A27**, 7647 (1994).

[57] F. Ritort (private communication).

[58] F. Ritort, Phys. Rev. **B55**, 14096 (1997).

[59] A. Barrat, R. Burioni and M. Mézard, J. Phys. A**29**, 1311 (1996). S. Franz and G. Parisi, J. Phys. I (France) **5**, 1401 (1995).

[60] L. F. Cugliandolo, D. R. Grempel and C. A. da Silva Santos, in preparation.

[61] L. F. Cugliandolo, D. R. Grempel, L. Ioffe, G. Lozano and C. da Silva Santos, in preparation.

[62] M. Mézard and G. Parisi, J. Phys. I (France) **2**, 2231 (1991). A. Engel, Nucl. Phys. **B410** [FS], 617 (1993).

[63] Y. Y. Goldschmidt, Phys. Rev. Lett. **74**, 5162 (1995).